Molecular Cancer

RESEARCH

Open Access

Exosomal circ_0006896 promotes AML progression via interaction with HDAC1 and restriction of antitumor immunity

Can Can[1†], Xinyu Yang[1,2†], Hexiao Jia[1], Hanyang Wu[1], Xiaodong Guo[1], Yihong Wei[1], Ziting Jia[1], Wancheng Liu[1], Amin Zhang[1], Na He[1], Hailei Zhang[1] and Daoxin Ma[1*]

Abstract

Background Drug resistance and immune escape continue to contribute to poor prognosis in AML. Increasing evidence suggests that exosomes play a crucial role in AML immune microenvironment.

Methods Sanger sequencing, RNase R and fluorescence in situ hybridization were performed to confirm the existence of circ_0006896. The role of circ_0006896 in the progression of AML was assessed by in vitro and in vivo functional experiments. Flow cytometry, RT-qPCR and adoptive T cell-transfer immunotherapy were conducted to assess the function of exosomal circ_0006896 in $CD8^+$ T cell dysfunction. RNA pull-down assay, mass spectrometry, immunofluorescence, co-immunoprecipitation and western blot were performed to identify and confirm the circ_0006896 interacting proteins.

Results CircRNA expression patterns in exosomes differ significantly between AML and controls compared to lncRNAs or mRNAs. A new crucial exosomal circRNA, circ_0006896, is upregulated in both AML cells and exosomes and correlates with the prognosis and relapse of AML. In vitro and in vivo studies suggest that circ_0006896 significantly promotes AML cell proliferation, reduces chemotherapy sensitivity, and more importantly, impairs the efficacy of adoptive T cell-transfer immunotherapy. Mechanistically, circ_0006896 physically interacts with the catalytic domain of histone deacetylase HDAC1, decreasing histone H3 acetylation, and impairing the transcription of genes involved in arachidonic acid metabolism, ultimately inhibiting lipid peroxidation and ferroptosis in AML cells. Exosomal circ_0006896 disrupts $CD8^+$ T cell function by interacting with HDAC1, impairing LEF1 transcription and subsequently decreasing the expression of cytotoxic molecules IFN-γ and Granzyme B.

Conclusions We demonstrate a self-driven progression mediated by exosomal circRNAs and $CD8^+$ T cells, highlighting the potential of targeting circRNAs in AML immunotherapy.

Keywords Acute myeloid leukemia, CircRNAs, Exosome, Arachidonic acid metabolism, Tumor microenvironment

†Can Can and Xinyu Yang contributed equally to this work.

*Correspondence:
Daoxin Ma
daoxinma@sdu.edu.cn
[1] Department of Hematology, Qilu Hospital of Shandong University, No.117, West of Wenhua Road, Jinan, Shandong 250012, People's Republic of China
[2] Department of Hematology, Shandong Provincial Hospital Affiliated to Shandong First Medical University, No.324, Jingwu Road, Jinan, Shandong 250021, People's Republic of China

Introduction

Acute myeloid leukemia (AML) is a heterogeneous and immunosuppressive malignancy characterized by uncontrolled expansion of immature myeloid cells and restricted differentiation of myeloid progenitor cells [1, 2]. Despite the availability of multiple targeted therapies in addition to standard induction chemotherapy, the 5-year survival rate remains below 30% due to drug resistance or rapid relapse, underscoring the urgent need for novel and synergistic treatments [3–5].

Recent studies have shown that leukemic cells create a unique niche by manipulating and altering the tumor microenvironment (TME), which directly enhances their survival and drug resistance. The TME in AML induces resistance to conventional chemotherapy and suppresses anti-tumor immune responses. Growing evidence has revealed that exosomes were primarily engaged in the crosstalk between leukemic cells and stroma cells or immune cells in TME by transferring biological components like proteins, metabolites, and nucleic acids [6, 7]. Exosomes from the AML cells not only directly promote leukemic progression but also dynamically remodel the bone marrow (BM) niche to a condition that is conducive to the proliferation and progression of leukemia cells. Increased RAB27B in leukemia stem cells (LSCs) has been reported to prevent their senescence, while exosomes from RAB27B-overexpressing LSCs induce senescence in mesenchymal stem cells (MSCs) [8]. AML-derived exosomes can induce MSCs to adopt an adipogenic differentiation propensity, which promotes leukemia cell engraftment [9]. Additionally, exosome-derived non-coding RNAs (ncRNAs) have been shown to impair the immune response of T cells and macrophages, creating an immunosuppressive microenvironment that drives AML progression [10, 11]. Among ncRNAs, circRNAs, due to their high stability and abundance, have unique advantages over other nucleic acids in intercellular transport. However, relatively little is known about the therapeutic potential of circRNAs in modulating the AML immune microenvironment.

CircRNAs have been identified as prognostic factors and potential therapeutic targets in AML progression [12, 13]. CircRNF220 [14] and circPLXNB2 [15] are highly expressed in AML and are associated with relapse and poor clinical outcomes in AML patients. Moreover, in our previous study, we demonstrated that specific circRNAs can enhance AML cell sensitivity to chemotherapy by acting as endogenous sponges for miR-499a-5p [16] or as molecular scaffolds between PRMT6 and histone H3 [17]. Post-translational modifications (PTMs) of histones are frequently mutated and deregulated in AML, contributing to the drug resistance of AML [18, 19]. Histone deacetylases (HDACs) participate in the dynamic regulation of histone deacetylation, thereby controlling downstream gene transcription [20]. HDAC1/3 is upregulated in refractory or relapsed AML cells, and combining HDAC inhibitors with chemotherapy can enhance the overall survival in these patients [21–23].

In this study, we identified a distinct expression pattern of circRNAs in AML exosomes and a leukemic promoting function of circ_0006896. Circ_0006896 inhibits lipid peroxidation-induced ferroptosis by binding HDAC1 in AML cells. Moreover, circ_0006896-enriched AML exosomes impair $CD8^+$ T cell cytotoxic function by interacting with HDAC1, thereby inducing an immunosuppressive microenvironment and promoting AML progression. Our findings reveal a novel role for circ_0006896 in AML chemoresistance and immune evasion through HDAC1-mediated epigenetic reprogramming, suggesting circ_0006896 as a potential therapeutic target in AML.

Materials and methods

Sample collection

Bone marrow mononuclear cells or supernatants were collected from newly diagnosed or relapsed non-M3 AML patients and healthy donors (HD) at Qilu Hospital of Shandong University between 2021 and 2023. The HD controls were individuals with only very slight anemia and without any morphological and genetic abnormality in the bone marrow. Supernatants were immediately frozen in liquid nitrogen after collection, while mononuclear cells were suspended in TRIzol and stored at −80 °C for subsequent RNA extraction. This study was conducted in accordance with the Declaration of Helsinki and was approved by the Ethics Committee of Qilu Hospital of Shandong University. The information of the patients used for the exosomal RNA transcriptome sequencing is listed in Supplementary Table 3.

RNA extraction and reverse transcription quantitative PCR (RT-qPCR)

Cellular total RNA and RNA from bone marrow supernatant exosomes were extracted by TRIzol reagent (Invitrogen, USA). RNA was reversely transcribed into cDNA using the M-MLV RTase cDNA Synthesis Kit (Takara Bio, Japan) according to the manufacturer's instructions. Real-time quantitative PCR (RT-qPCR) was performed using 2×SYBR Green qPCR Mix (Spark Jade, China) on Roche LightCycler 480 System (Roche Applied Science, USA). The PCR reaction mixture had a final volume of 10μL, including 1 μL of cDNA, 3μL of RNase Free H_2O, 5 μL of 2×SYBR Green qPCR Mix and 0.5 μL of the forward and reverse primers. The expression of targeted genes was calculated using the $2^{-\triangle CT}$ or $2^{-\triangle\triangle CT}$

method. The primers used for the detection were listed in Supplementary Tables 4, 5.

RNase R treatment

A total of 3 μg RNA was digested with 12 U RNase R (Beyotime, China) at 37 °C for 15 min, followed by incubation at 70 °C for 10 min. The remaining RNA was further analyzed with RT-qPCR.

DNA agarose gel electrophoresis and Sanger sequencing assay

Genomic DNA (gDNA) or cDNA was amplified using divergent and convergent primers specific for circ_006896. PCR products were analyzed by 5% agarose gel electrophoresis. Meanwhile, the amplified products were subjected to Quick Shot Sanger Sequencing (Boshang, China) to ascertain the head-to-tail splicing.

RNA fluorescence in situ hybridization (FISH)

RNA fluorescence in situ hybridization was performed using an RNA FISH Kit (GenePharma, China) according to the manufacturer's instructions. A Cy3-labeled probe specific to the circ_006896 sequence was obtained from GenePharma. Briefly, cells were fixed and dropped onto a slide with 4% paraformaldehyde at room temperature followed by permeabilization with 0.1% Triton X-100. After overnight hybridization with 5 μL probes in prehybridization buffer at hybridizer, the slides were washed as indicated in the instruction and counterstained with DAPI-Aqueous, Fluoroshield (Abcam, UK). Images were captured using an LSM900 Laser Confocal Microscope (Carl ZEISS, Germany). The sequence of the circ_006896 probe: GAT GTC TCT CTT TCA GTT AGG TCT A; antisense probe: TAG ACC TAA CTC AAA GAG AGA CAT C.

Exosome extraction

AML cells were cultured in RPMI-1640 medium supplemented with exosome-depleted fetal bovine serum (FBS) for 48 h. The exosomes were extracted by differential ultracentrifugation. Briefly, the supernatants from cell culture medium or bone marrow were centrifuged at 300 g for 10 min to remove cells, and filtered through 0.22 μm filter, followed by 2000 g 10 min to remove dead cells, 10000 g 30 min to remove cell debris, and 100000 g 70 min to purify exosomes. The pellets were resuspended in PBS for further experiments and identification. Particle morphology was identified via transmission electron microscope. Exosome size was detected by nanoparticle tracking analysis (NTA) and the protein markers were determined by western blot.

PKH67 labeling of exosomes

To observe the uptake of exosomes by AML cells or T cells, exosomes were labeled with the PKH67 fluorescent cell linker kit (Sigma–Aldrich, USA). Exosomes or 4μL of PKH67 were dissolved in 1 mL Diluent C solution for 5 min, mixed and incubated for another 5 min. After neutralization with an equal volume of 0.5% BSA solution, the exosomes were centrifuged at 100,000 g for 1 h and resuspended in PBS for further study.

Cell culture

The human AML cell lines (THP-1, Molm-13 and U937), as well as 293 T, were obtained from the Cell Bank of China Center for Type Culture Collection (Shanghai, China). THP-1, Molm-13, and U937 were cultured in RPMI-1640 medium (Gibco, USA) supplemented with 10% FBS (Bio-channel, China) and 1% penicillin/streptomycin (P/S, New Cell & Molecular Biotech, China). 293 T cells were cultured in DMEM (Gibco, USA) with 10% FBS and 1% P/S. All cells were cultured in a humidified atmosphere at 37 °C containing 5% CO_2.

Cell transfection

For stable transfection, lentivirus containing short hairpin RNA (shRNA) targeting circ_006896 or lentivirus containing circ_006896 overexpressing plasmid was transfected into cells in the presence of Polybrene (Gene Pharma, China). 48 h after the transfection, the cells were observed by fluorescence microscope and were selected with puromycin and expanded until use. For transient transfection, shRNA of circ-0006896 or FLAG-tagged truncation expression plasmid for HDAC1 (Boshang, China) was transfected with Lipofectamine 2000 reagent (Thermo Fisher Scientific, USA) following the manufacturer instructions. The lentivirus, shRNAs and plasmid were produced by Gene Pharma. Negative Control: S: UUC UCC GAA CGU GUC ACG UTT, AS: ACG UGA CAC GUU CGG AGA; shRNA1: S: GAC CUA ACU CAA AGA GAG ATT, AS: UCU CUC UUU GAG UUA GGU CTT; shRNA2: S: CCU AAC UCA AAG AGA GAC ATT, AS: UGU CUC UCU UUG AGU UAG GTT. Overexpression lentivirus: AGAGACATCTCCCCATACATT TCAAT.

Cell proliferation and viability assays

Cell proliferation and viability were assessed using the CCK-8 assay (Bestbio, China). A total of 1×10^4 cells in 100μL of medium were seeded into 96-well plates and cultured for 0, 24, 48 h and 72 h. Then, 10μL CCK-8 was added to each well and incubated for 4 h, after which the

optical density (OD) value was measured by microplate reader (Biotek, Synergy H1, Vermont, USA).

Cell apoptosis and death assay

Cell apoptosis was determined by the Annexin V-FITC/PI or Annexin V-Alexa Fluor 660/7-AAD apoptosis detection kit (Bestbio, China). Briefly, cells were harvested, washed with PBS twice, and incubated in Annexin V binding buffer with Annexin V-FITC/PI for 15 min (or with Annexin V-Alexa Fluor 660 /7-AAD for 10 min) at 4 °C in the dark. Cell death was also determined by the PI staining (Bestbio, China) for 5 min at 4 °C in the dark and analyzed by flow cytometry.

RNA pull-down assay

RNA pull-down assay was performed using Pierce™ Magnetic RNA–Protein Kit (Thermo Fisher Scientific, USA). Cell lysates were incubated overnight with 50 pmol biotin-conjugated circ_006896 probe. Then, the cell lysates were incubated with Pierce Nucleic-Acid Compatible Streptavidin Magnetic Beads at 4℃ for 1 h. After washing, the magnetic beads were analyzed for potential binding proteins using mass spectrometry and western blot. The specific biotin-conjugated pull-down probes and anti-probe were synthesized by GenePharma. Anti-probe: TAG ACC TAA CTC AAA GAG AGA CAT C; Probe 1: GAT GTC TCT CTT TCA GTT AGG TCT A; Probe 2: TGG GGA GAT GTC TCT CTT TGA GTT A.

Silver stain assay

Potential circ_006896-binding proteins were pulled down using a specific probe and were separated with 10% SDS polyacrylamide gels. Proteins in the gel were stained with Pierce Silver Stain Kit (Thermo Fisher Scientific, USA) according to the manufacturer's instructions.

Co-immunoprecipitation (Co-IP)

AML cells (2×10^7) were lysed and incubated with 2 μg antibody or control IgG at 4℃ overnight with agitation. The lysates were then incubated with 20 μL protein A/G magnetic beads (Thermo Fisher Scientific, USA) for 1 h at room temperature. After washing with TBST, the target protein bound to magnetic beads was detected by western blot.

Western blot analysis

A total of 30 μg of protein was separated by SDS-PAGE gel and transferred to a PVDF membrane (Millipore, USA). After blocking with 5% skim milk at room temperature for 1 h, the membranes were incubated overnight at 4 °C with the primary antibodies: H3 (Proteintech, 68,345–1-Ig), HDAC1 (Proteintech, 66,085–1-Ig), Ac-H3K9 (Cell Signaling Technology, 9649S), Ac-H3K27 (Cell Signaling Technology, 8173 T), GAPDH (Proteintech, 60,004–1-Ig), HDAC2 (HUABIO, ET1607-78), HDAC3 (HUABIO, ET1610-5), Flag (Proteintech, HRP-66008), Calnexin (Proteintech, 10,427–2-AP), Tom20 (Proteintech, 11,802–1-AP), CD63 (Proteintech, 67,605–1-Ig), and TSG101 (Proteintech, 67,381–1-Ig). After washing three times with TBST buffer, the membranes were incubated with relevant HRP-conjugated secondary antibodies (CST, 7074, 7076) at room temperature for 1 h. Proteins were visualized by SageCapture Chemiluminescent Imaging System (ChampChemi 610 Plus, China) using ECL hypersensitive developer (Abbkine, China).

Immunofluorescence (IF)

AML cells were fixed with 4% paraformaldehyde and applied onto a poly-L-lysine-coated slide. Slides were permeabilized with 0.1% Triton X-100 and then blocked with 10% donkey serum. Primary antibodies against HDAC1 and histone H3 were incubated simultaneously in a humidifying chamber overnight. After washing with PBS, slides were incubated with fluorescently conjugated secondary antibodies for 2 h at room temperature. Slides were mounted with DAPI-Aqueous, Fluoroshield for confocal fluorescence microscopy.

RNA immunoprecipitation (RIP) assay

RIP assay was conducted using Magna RIP RNA-binding Protein Immunoprecipitation Kit (Millipore, USA) following the manufacturer's instructions. Briefly, cells (1×10^7) were lysed in RIP lysis buffer containing protease inhibitor cocktail and RNase inhibitors. Magnetic beads were coated with certain antibody or IgG. The cell lysates were incubated with the antibodies-coated magnetic beads at 4 °C overnight. Then, the co-precipitated RNAs were purified in proteinase K buffer and extracted using phenol: chloroform: isoamyl alcohol (25:24:1). Immunoprecipitated RNA was then analyzed by RT-qPCR. The enrichment values were normalized to input control and IgG isotype control.

Chromatin immunoprecipitation (ChIP) assay

ChIP analysis was performed using Simple ChIP® Enzymatic Chromatin IP Kit (CST, USA) according to the manufacturer's instructions. Cells were cross-linked with 1% formaldehyde for 10 min. Nuclei were extracted and the chromatin was digested with micrococcal nuclease, and the nuclear membrane was disrupted by sonication. The diluted chromatin samples were incubated with HDAC1 or IgG antibodies overnight at 4 °C. Then 30 μl of magnetic beads were added to each reaction and incubated at 4 °C for 2 h. The chromatin was eluted from the magnetic beads with ChIP elution buffer. The cross-links were reversed by digestion with proteinase K and the

eluted DNA was purified with spin columns. Enriched DNA was analyzed by PCR with promoter region primers of the targeted genes.

Arachidonic acid metabolite sequencing and ELISA

About 1×10^7 cells were used to determine arachidonic acid and its metabolites. The lysed samples were separated by Agilent 1290 Infinity UPLC, and then were applied for mass spectrometry analysis by using 6500/5500 QTRAP. 5-Hydroxyeicosatetraenoic Acid (5S-HETE) levels in the cells were measured using the Human 5S-HETE ELISA Kit (Cusabio, China). Briefly, an equal number of cells from different groups were lysed by freeze-thawing with liquid nitrogen. Solutions were centrifuged at 12,000 g for 15 min at 4 °C and the supernatants were collected for further ELISA analysis according to the manufacturer's instructions.

ROS and BODIPY 581/591 C11 detection

Cellular ROS was measured using DCFH-DA (Beyotime, China) and the lipid peroxidation was assessed using BODIPY 581/591C11 (Invitrogen, USA). Cells in different groups were harvested and incubated with DCFH-DA at a 1:1000 dilution or 5 μM BODIPY 581/591 C11 at 37℃ for 20 min followed by three times wash with incomplete culture medium. The mean fluorescence intensities of ROS and BODIPY C11 were analyzed by flow cytometry.

Malondialdehyde (MDA) detection

The levels of MDA were evaluated by MDA Assay Kit (Solarbio, China) following the manufacturer's instructions. The MDA was extracted with MDA extraction solutions by freeze and thaw cycling in nitrogen. The supernatants were mixed with working solutions and incubated at 100℃ for 1 h. Then the absorbance values were then measured at 532 nm and 600 nm.

Isolation and activation of $CD8^+$ T cells

The peripheral blood mononuclear cells (PBMCs) were isolated using Ficoll solution (tbdscience, China) according to the manufacturer's instructions. $CD8^+$ T cells were sorted from the PBMCs by CD8 magnetic beads (MiltenyiBiotec, Germany). $CD8^+$ T cells were activated using anti-CD3 (2 μg/mL) and anti-CD28 (2 μg/mL) (Biolegend, USA) antibodies and 100 IU/mL rhIL-2 (PeproTech, USA) for 24 h. Then they were transfected with shRNA for further experiments. Apoptosis and the differentiation of $CD8^+$ T cells were then analyzed by flow cytometry.

Dendritic cells (DCs) and tumor-specific T cell activation

Tumor-specific T cells were activated as described in a previous study [24]. Isolated PBMCs were cultured in RPMI-1640 medium supplemented with 1% FBS for 1 h, after which non-adherent cells were removed. The remaining adherent monocytes were cultured with 100 ng/mL GM-CSF (PeproTech, USA) and 20 ng/mL IL-4 (PeproTech, USA) for 5 days. Half of the medium was replaced with fresh medium containing the same cytokines every two days. After 5 days, DCs were then primed with 10 ng/mL TNF-α (PeproTech, USA) and 100 μg/mL Molm-13 cell lysates to induce maturation and generation of tumor-antigen loaded DCs. $CD8^+$ T cells isolated from the same donors were then co-cultured with the primed DCs supplemented with 50 IU/ml rhIL-2 (PeproTech, USA) and exosomes (10 μg/mL protein concentration) for 3 days to generate tumor-specific T cells.

$CD8^+$ T cells detection

$CD8^+$ T cells were incubated with 100 ng/mL PMA (BioGems, USA), 1 μg/mL ionomycin (BioGems, USA) and 10 μg/mL BFA (BioGems, USA) in complete medium for 4 h, then stained with surface marker and intracellular proteins markers by FIX&PERM kit (Multiscience Lianke, China) according to the manufacturer's instructions. Briefly, cells were stained with CD8 antibodies at 4℃ for 30 min and then fixed with buffer A for 15 min at room temperature, washed and incubated with the intracellular protein antibodies in buffer B at 4℃ for 30 min. Cell differentiation was analyzed using a Beckman Gallios cytometer. Following antibodies were used for staining $CD8^+$ T cells, anti-human CD45-PE (Invitrogen, 12–0459-42), CD8-PerCP/Cy5.5 (Biolegend, 344,710), CD8-APC/Cy7 (Biolegend, 344,714), IFN-γ-FITC (Invitrogen, 11–7319-82), TNF-α-APC (Invitrogen, 17–7349-82), and Granzyme B-PE (Invitrogen, GRB04).

Mouse xenograft model

Male NOG mice (5–6 weeks old) from Vital River Laboratory Animal Technology (China) were used for human cell-derived xenograft transplantation experiments. AML cells transfected with sh-circ or NC-circ were suspended in normal saline and injected into mice via tail vein at the following concentration (THP-1, 1×10^7/100μL per mouse; Molm-13, 3×10^6/100μL per mouse). 20 μg extracted exosomes were injected intravenously every 3 days, starting 2 weeks after THP-1 injection. Additionally, 5 days after injection of Molm-13 cells, mice were treated with 10 mg/kg chidamide by oral gavage every other day and sacrificed upon signs of distress.

For adoptive cell-transfer therapy, $CD8^+$ T cells isolated from PBMCs of healthy donors were activated with DC cells and then incubated with the sh-circ or NC-circ exosomes for 48 h. Five days after the injection of Molm-13 cells, 3×10^6/100μL $CD8^+$ T cells were intravenously injected into leukemia-bearing mice via the tail vein. The day after $CD8^+$ T cells injection, mice were treated with 10 mg/kg chidamide or vehicle (DMSO + corn oil) by oral gavage every other day. Disease symptoms were monitored daily. GFP^+ leukemic cells or immune cells in bone marrow, spleen, and peripheral blood were analyzed by flow cytometry.

Statistical analysis

All the data are presented as mean ± standard deviation (SD) unless otherwise stated. Data were analyzed using GraphPad Prism 8.0 (GraphPad Software Inc., USA) and SPSS 25 software (IBM, USA). Statistical significance was determined by Student's t-test, paired t-test and One-way or Two-way ANOVA with multiple comparisons for data conforming to normal distribution and homogeneity of variance. Expression data that do not conform to normal distribution were assessed with Mann–Whitney U tests. Chi-square test or Fisher's exact test was applied for the comparison of clinical data. Pearson's correlation coefficient was used to analyze statistical correlation. Survival analysis was performed using Log-rank test. $P < 0.05$ were considered statistically significant.

Results

Exosome-derived circ_0006896 is upregulated in AML patients and correlates with poor prognosis

To investigate the role of AML-derived exosomes in AML progression, we first isolated exosomes from the bone marrow supernatant of 6 AML patients and 4 healthy donors using differential ultracentrifugation. The morphology and size of the isolated exosomes were determined by using transmission electron microscopy and NTA analysis (Fig. 1A). Then, we performed RNA transcriptome sequencing on exosomes (Fig. 1B, Supplementary Fig. 1A) and identified 4296 differentially-expressed circRNAs, 2173 differentially-expressed mRNAs and 29,950 differentially-expressed lncRNAs (|log2(Fold Change) |> 2.0, *P*-value < 0.05). Notably, sample expression clustering and principal component analysis showed that the expression pattern of circRNAs was significantly different between AML patients and HD controls compared to those of mRNAs or lncRNAs (Supplementary Fig. 1B). Our results indicate that circRNAs might serve as a much more sensitive biomarker than mRNAs or lncRNAs in AML exosomes.

As we previously identified differentially expressed circRNAs in AML cells [16, 17] and confirmed their involvement in AML progression, we integrated the two datasets for cross-analysis. We identified 500 significantly upregulated circRNAs in AML-derived exosomes, with only 5 circRNAs showing simultaneous upregulation in both AML cells and exosomes (GSE94591) (Fig. 1C). Then, we designed and synthesized primers of the 5 circRNAs (hsa_circ_0006896, hsa_circ_0029633, hsa_circ_0000825, hsa_circ_0012152 and hsa_circ_0002805) for detection in a larger sample of bone marrow samples. Our results showed that all five circRNAs were consistent with the microarray results, among which hsa_circ_0006896 had the highest fold change in both AML cells and exosomes (Fig. 1D). Further validation of hsa_circ_0006896 in another dataset, GSE163386, also confirmed its higher expression in AML patients (Supplementary Fig. 1C). Hsa_circ_0006896, derived from KIAA1429 and designated as circ_0006896, was found to be significantly upregulated in both AML cells and exosomes, with higher expression in relapsed AML than in newly diagnosed cases (Fig. 1E). Pearson correlation analysis of the same cohort showed a significant correlation between exosomal circ_0006896 expressions and its cellular expressions (Supplementary Fig. 1D). Ultimately, circ_0006896 was selected for further investigation.

Circ_0006896 is a 136-nt circRNA generated from the exons 22–23 of m6A methyltransferase KIAA1429 gene located on chr8:95,549,330–95550574. The head-to-tail

(See figure on next page.)

Fig. 1 Identification and validation of circ_0006896 in AML cells and exosomes. **A** Representative electron micrograph and NTA analysis of exosomes isolated from AML patients' bone marrow. **B** Heatmap of differentially expressed circRNAs in bone marrow exosomes from healthy donors and AML patients. **C** Schematic diagram illustrating the screening of candidate circRNAs in AML. **D** Cellular and exosomal expression of candidate circRNAs in AML patients ($n = 9$) and healthy donors ($n = 4$). Statistical data were presented in median with range and analyzed with Mann–Whitney U tests. **E** Circ_006896 shows significantly higher expression in newly diagnosed and relapsed AML bone marrow cells and exosomes compared to healthy donors. Statistical data were presented in violin plot and analyzed by nonparametric One-Way ANOVA and multiple comparisons. **F** Genomic position and splicing mode of circ_0006896. The backsplice site was confirmed by Sanger sequencing. **G** Agarose gel electrophoresis showing the amplification of circ_0006896 in cDNA or gDNA using convergent and divergent primers. **H** mRNA expression of circ_0006896 and KIAA1429 after treatment with RNase R. Statistical data were analyzed by Student's t-test. **I** RNA FISH analysis showing the localization of circ_0006896 in AML cells (Scale bar = 20 μm). Statistical data were presented in mean ± SD unless otherwise stated, $^*P \le 0.05$, $^{**}P \le 0.01$, $^{***}P \le 0.001$, $^{****}P \le 0.0001$ and ns indicates $P > 0.05$

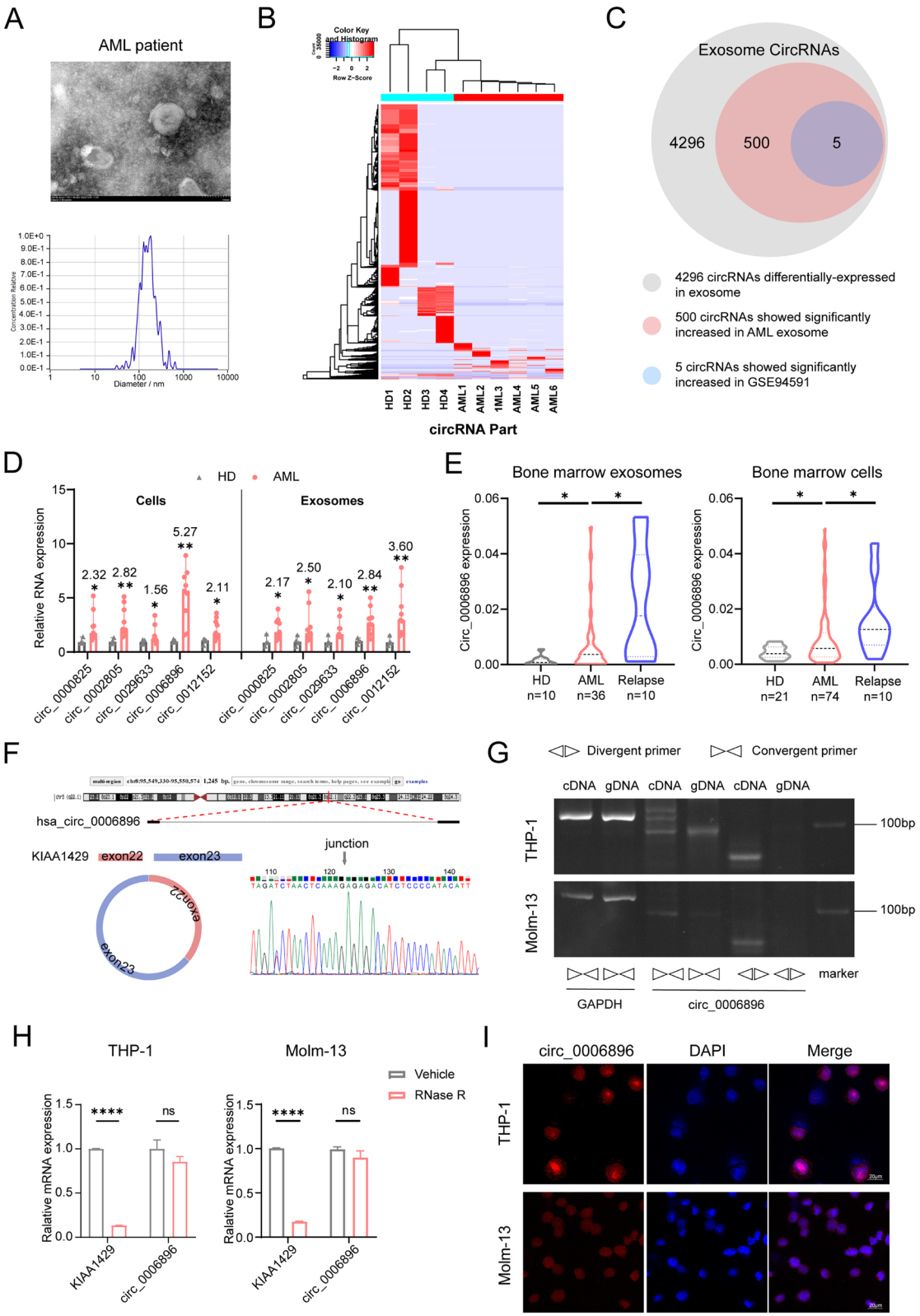

Fig. 1 (See legend on previous page.)

splice junction of circ_0006896 was successfully amplified by RT-qPCR and confirmed by Sanger sequencing, and the sequence is consistent with circBase database annotation (http://www.circbase.org/) (Fig. 1F). We also found that circ_0006896 could be amplified by divergent primers in cDNA but not in genomic DNA, further confirming that it is derived from backsplice instead of trans-splicing or genomic rearrangements (Fig. 1G). Moreover, resistance to RNase R exonuclease digestion confirmed that circ_0006896 forms a closed loop structure (Fig. 1H). Furthermore, the results of RNA FISH demonstrated that circ_0006896 was localized in both cytoplasm and nucleus of AML cells (Fig. 1I). In summary, these results demonstrate the presence of a new circ_0006896 in AML cells.

As for clinical relevance, we further demonstrated that AML patients with higher exosomal circ_0006896 expressions had a significantly poorer prognosis than those with lower circ_0006896 expressions (Supplementary Table 1, 2). Importantly, receiver operating characteristic (ROC) curve analysis showed that circ_0006896 in both AML cells and exosomes has diagnostic value for distinguishing AML patients from healthy individuals, and exosomal expression shows greater sensitivity (Supplementary Fig. 1E). Overall, our results suggest that circ_0006896 is upregulated in both AML-derived exosomes and AML cells, and positively correlates with AML progression.

Exosome-derived circ_0006896 is responsible for exosome-induced AML progression

To explore the role of circ_0006896 in AML progression, we determined the endogenous expression and exosomal secretion of circ_0006896 in 5 commonly used AML cell lines and selected the highly-expressed THP-1 and Molm-13 cells for the following experiments (Supplementary Fig. 2A). Furthermore, we synthesized two shRNAs targeting the backsplice junction region and constructed a circ_0006896 overexpressing plasmid. After transfection, our results confirmed that the circ_0006896 expression in AML cells was efficiently knocked down or overexpressed (Supplementary Fig. 2B). We also proved that knockdown or overexpression of circ_0006896 did not alter the mRNA level of linear KIAA1429 (Supplementary Fig. 2C).

Subsequently, in vitro studies showed that knockdown of circ_0006896 inhibited AML proliferation, increased cell apoptosis, and enhanced AML cells drug sensitivity to IDA (Fig. 2A, C, Supplementary Fig. 2D, G). In contrast, circ_0006896 overexpression significantly promoted AML cell proliferation, decreased cell apoptosis, and reduced AML cells drug sensitivity to IDA (Fig. 2B, Supplementary Fig. 2E, F, H). Furthermore, we downregulated circ_0006896 in primary AML patient cells. Our result showed that the knockdown of circ_0006896 significantly inhibited the cell viability and promoted the apoptosis of primary AML cells (Fig. 2D, E). To determine whether circ_0006896 knockdown could inhibit AML progression in vivo, we established a xenotransplantation AML mouse model by intravenously injecting sh-circ_0006896-transfected THP-1 or Molm-13 cells into NOG mice. The results showed that circ_0006896 knockdown significantly inhibited AML progression in mice. Flow cytometry analysis revealed that the percentage of leukemia cells in the bone marrow and spleen of sh-circ_0006896 AML mice was significantly lower than in control AML mice. Additionally, spleen weight in sh-circ_0006896 mice was significantly lower than that in the control group. Importantly, survival analysis showed that sh-circ_0006896 AML mice had a significantly longer lifespan than control AML mice (Fig. 2F, G). In conclusion, these results suggest that circ_0006896

(See figure on next page.)

Fig. 2 Intracellular and exosomal circ_0006896 promote AML proliferation and chemotherapy sensitivity in vivo and in vitro. **A**, **B** Proliferation of AML cells transfected with shRNAs or overexpressing plasmid of circ-0006896. Statistical data were analyzed with Two-Way ANOVA and multiple comparisons. **C** Apoptosis of AML cells after transfection with shRNAs. Statistical data were analyzed with One-Way ANOVA and multiple comparisons. **D** Proliferation of primary AML cells transfected with shRNA. Statistical data were analyzed with Two-Way ANOVA and multiple comparisons. **E** Apoptosis of primary AML cells after transfection with shRNA. Statistical data were analyzed by paired Student's t-test. **F**, **G** Spleen weight, leukemic burden and survival analysis of NOG mice injected with circ_0006896 knockdown cells ($n=5$ or $n=4$). Statistical data were analyzed by Student's t-test. **H** Proliferation of AML cells incubated with exosomes from circ_0006896-upregulated or -downregulated cells. Statistical data were analyzed with Two-Way ANOVA and multiple comparisons. **I** Apoptosis of THP-1 cells incubated with exosomes from circ_0006896-upregulated or -downregulated cells. Statistical data were analyzed by Student's t-test. **J** Proliferation of THP-1 cells incubated with exosomes from circ_0006896-downregulated cells and exosomes blocker, GW4869 (10 μM, Beyotime, China). Statistical data were analyzed with Two-Way ANOVA and multiple comparisons. **K** Apoptosis of THP-1 cells incubated with exosomes from circ_0006896-downregulated cells and exosomes blocker, GW4869. Statistical data were analyzed by Student's t-test. **L**, **M** Leukemic burden of mice treated with exosomes from circ_0006896 downregulated THP-1 cells ($n=3$). Statistical data were analyzed with One-Way ANOVA and multiple comparisons. **N** Representative image and spleen weight of mice treated with exosomes from circ_0006896 downregulated THP-1 cells ($n=3$). Statistical data were analyzed with One-Way ANOVA and multiple comparisons. Statistical data were presented in mean ± SD, $^{*}P \le 0.05$, $^{**}P \le 0.01$, $^{***}P \le 0.001$, $^{****}P \le 0.0001$ and ns indicates $P > 0.05$

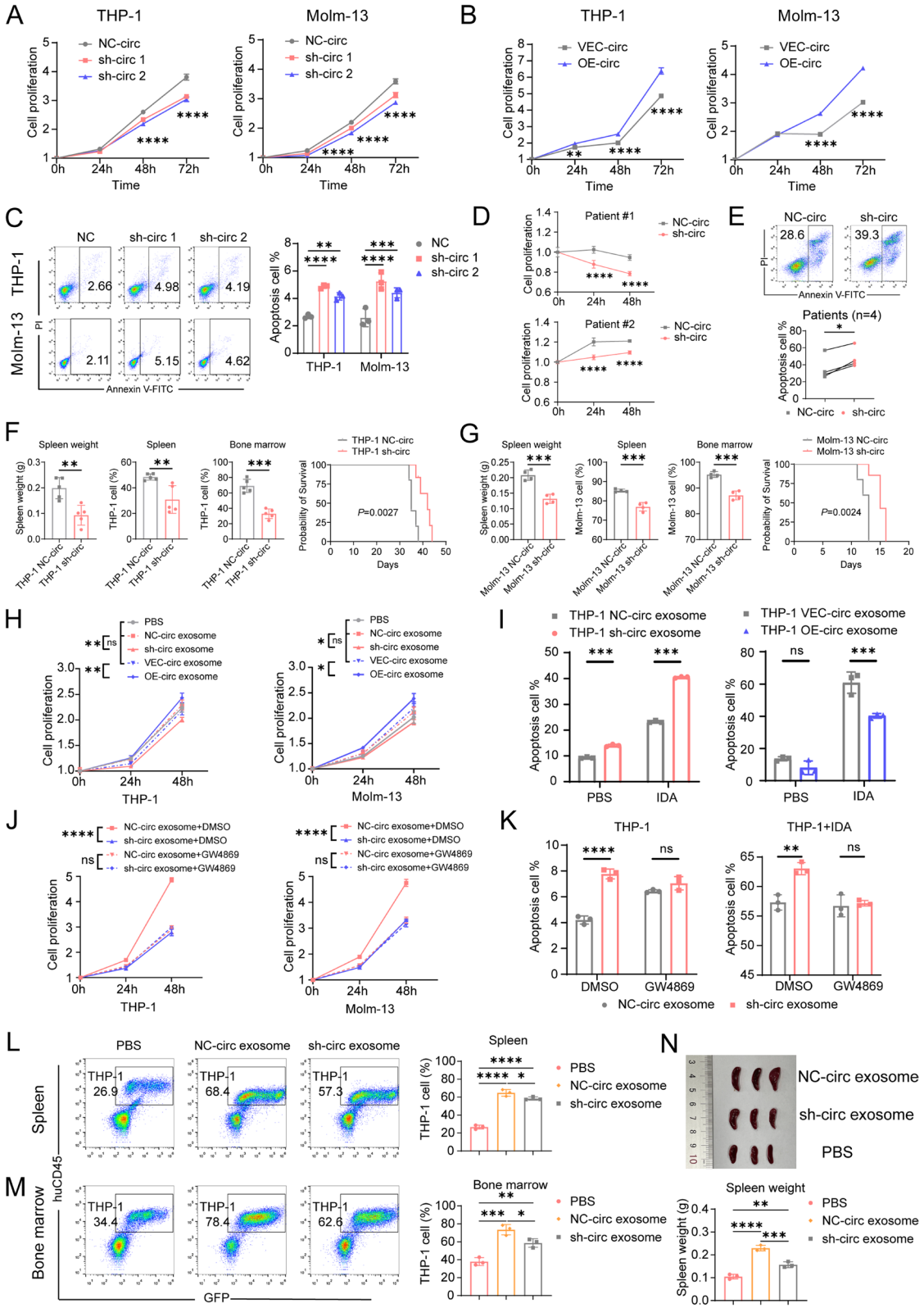

Fig. 2 (See legend on previous page.)

knockdown suppresses AML progression both in vitro and in vivo.

Recent studies have shown that tumor-derived exosomes play important and fundamental roles in tumor progression [25, 26]. Considering the enrichment of circ_0006896 in AML exosomes, we further investigated whether circ_0006896 plays a role in AML progression by being loaded into exosomes. We first isolated exosomes from THP-1 or Molm-13 cells and confirmed their characteristics using western blot, NTA and TEM (Supplementary Fig. 2I, J). Confocal microscopy analysis showed that AML-derived exosomes labeled with PKH67 were readily absorbed by AML cells (Supplementary Fig. 2 K). Then, RT-qPCR analysis revealed that circ_0006896 level in exosomes derived from sh-circ_0006896 AML cells was significantly downregulated, while that in exosomes derived from circ_0006896-overexpressing AML cells was much higher (Supplementary Fig. 2L). We then incubated AML cells with exosomes isolated from these cells. The results showed that circ_0006896-overexpressing exosomes significantly promoted AML cell proliferation, decreased apoptosis, and reduced drug sensitivity compared to control exosomes (Fig. 2H, I, Supplementary Fig. 2M). Conversely, opposite effects were found when circ_0006896-downregulated exosomes were applied (Fig. 2H, I, Supplementary Fig. 2M). More importantly, the proliferation inhibitory, apoptosis enhancing and drug sensitivity increasing effects of the circ_0006896-downregulated exosomes were significantly suppressed when GW4869, an exosome blocker, was applied (Fig. 2J, K, Supplementary Fig. 2N). The similar suppressing effects on cell proliferation were observed when GW4869 was used as an additional control in cells treated with circ_0006896-overexpressing exosomes (Supplementary Fig. 2O). Additionally, the xenotransplantation AML mouse model was successfully established, followed by intravenous injection of exosomes. The results showed that AML exosomes significantly promoted AML progression compared to PBS treatment, while knockdown of circ_0006896 significantly suppressed this effect. The percentages of leukemia cells in the bone marrow and spleen were substantially increased in mice treated with AML exosomes, but this could be alleviated by circ_0006896 knockdown (Fig. 2L, M). Similar results were observed for spleen weight (Fig. 2N). These experiments demonstrated that exosomal circ_0006896 was the essential participant in exosome-induced AML progression.

Circ_0006896 promotes AML by physically binding to HDAC1, decreasing histone acetylation levels

Studies have reported that circRNAs usually function as competing endogenous RNAs (ceRNAs) or scaffolds for RNA-binding proteins (RBPs). To investigate whether circ_0006896 regulates target genes by miRNA sponge, we performed an RIP assay. Our results showed that circ_0006896 was not pulled down by the AGO2 antibody in AML (Supplementary Fig. 3A), suggesting that circ_0006896 may not act as a miRNA sponge in AML cells. To determine whether circ_0006896 exerts its function by directly interacting with proteins, we designed two different circ_0006896 biotin probes and performed an RNA pull-down assay followed by a mass spectrometry assay to identify the associated proteins. A total of 69 proteins were found to bind to two different sense probes simultaneously, but not to the anti-sense probe (Supplementary Table 7). Similarly, the identified proteins did not include AGO2, further confirming that circ_0006896 does not act as a miRNA sponge in AML. Interestingly, among these proteins, the obvious binding of circ_0006896 on HDAC1 protein was observed in both sense probes. Given that HDAC1, a key molecule involved in AML epigenetic regulation, is a well-known histone deacetylase in many cancers, we thus focused on whether and how circ_0006896 regulates HDAC1 to promote AML progression. We first validated the interaction

(See figure on next page.)

Fig. 3 Circ_0006896 promotes AML by physically interacting with HDAC1 and inducing the deacetylation of histone H3. **A**, **B** Western blot of HDAC1 in circ_0006896 RNA pull-down proteins and circ_0006896 enrichments in HDAC1 RIP assay. Statistical data were analyzed by Student's t-test. **C** Co-localization of circ_0006896 and HDAC1 visualized by RNA FISH and immunofluorescence. Green indicated HDAC1, red indicated circ-0006896 (Scale bar = 2 μm). **D**, **E** Western blot of Ac-H3K27 and Ac-K3K9 in circ_0006896-downregulated or -upregulated AML cells. **F** Western blot of indicated proteins in HDAC1 or histone H3 immunoprecipitated complexes from lysates of Molm-13 cells. **G** Representative IF images identifying co-localization of HDAC1 and H3 in circ-0006896 downregulated AML cells. Purple indicated HDAC1, yellow indicated the H3 (Scale bar = 5 μm). **H** Schematic representation of HDAC1 functional domains and corresponding truncation constructs. **I**, **J** RIP and RNA pull-down assay of 293 T cells transfected with full-length HDAC1 or the indicated truncation constructs. Statistical data were analyzed by Student's t-test. **K** Proliferation of circ_0006896 knockdown AML cell lines and primary AML cells synergized with chidamide (4 μM). Statistical data were analyzed with Two-Way ANOVA and multiple comparisons. **L** Schematic overview of the experimental design for chidamide treatment (10 mg/kg) on NOG mice injected with Molm-13 cells ($n = 5$). **M** Representative image and spleen weight of mice treated with chidamide. Statistical data were analyzed by Student's t-test **N** Leukemic burden of mice treated with chidamide. Statistical data were analyzed by Student's t-test **O** Kaplan–Meier curves analysis showing the synergistic effect of sh-circ and chidamide on AML mice survival ($n = 5$). Statistical data were presented in mean ± SD, $^{*}P \le 0.05$, $^{**}P \le 0.01$, $^{***}P \le 0.001$, $^{****}P \le 0.0001$ and ns indicates $P > 0.05$

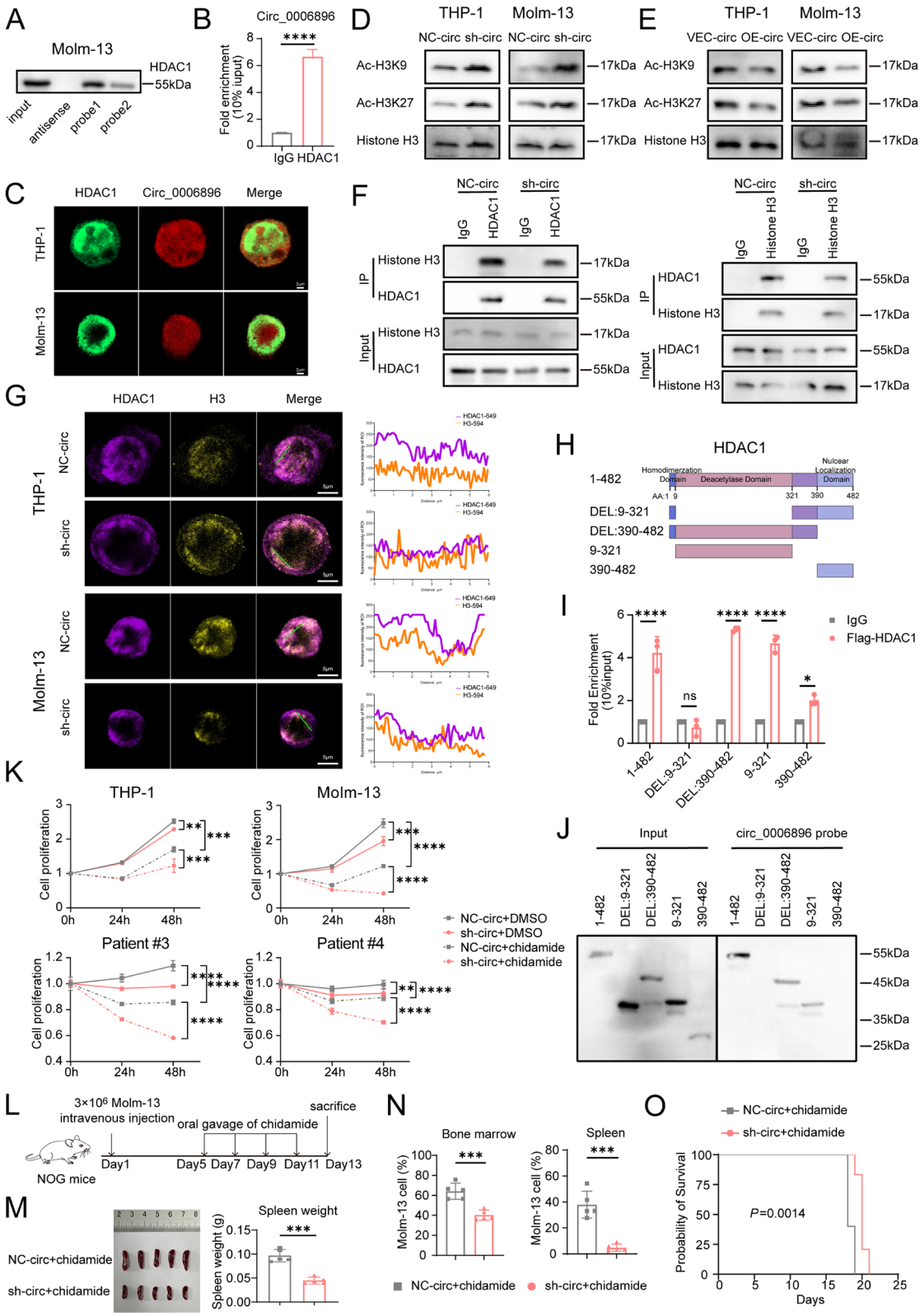

Fig. 3 (See legend on previous page.)

between circ_0006896 and HDAC1 using western blot and RIP analysis (Fig. 3A, B). Moreover, the immunofluorescence and RNA FISH analysis further demonstrated that circ_0006896 co-localizes with HDAC1 in the nucleus (Fig. 3C). The results of pull-down assay also showed that HDAC2 and HDAC3 could not be pulled down by the circ_0006896 probe, indicating the specificity of HDAC1 as a target (Supplementary Fig. 3B). RT-qPCR and western blot results also showed that the mRNA expression and protein level of HDAC2 and HDAC3 was not affected when circ_0006896 was downregulated (Supplementary Fig. 3C, D). All these results indicated that HDAC1, but not other HDACs, is the specific target of circ_0006896.

The aforementioned results prompted us to investigate how circ_0006896 regulates HDAC1 function. Our results of RT-qPCR and western blot assays showed that circ_0006896 did not significantly alter the mRNA or protein level of HDAC1 (Supplementary Fig. 3E, F). CircRNAs are known to function as scaffolds for proteins, facilitating efficient target recognition. Therefore, we speculated that circ_0006896 might serve as a scaffold for RBPs to regulate HDAC1 and further influence the deacetylation of histone rather than regulating its expression. Therefore, we next explored whether histone deacetylase activity of HDAC1 depends on the presence of circ_0006896. Our results showed that knockdown of circ_0006896 led to a significant increase in H3K9 and H3K27 acetylation, while overexpressed circ_0006896 led to a significant decrease in H3K9 and H3K27 acetylation (Fig. 3D, E). We then performed a Co-IP assay to examine whether circ_0006896 functions as a scaffold to enhance the binding of HDAC1 with histone. Our results showed that knockdown of circ_0006896 remarkably weakened the binding of HDAC1 to histone H3 (Fig. 3F). Meanwhile, immunofluorescence analysis showed reduced co-localization of HDAC1 and histone H3 in sh-circ_0006896 AML cells compared to control AML cells (Fig. 3G). To identify the specific domains required for HDAC1-circ_0006896 interactions, we constructed HDAC1 deletion mutants based on its domain structure (Fig. 3H). The results of RIP-qPCR and pull-down assays revealed that the catalytic domain of HDAC1 was the crucial domain for the interaction between HDAC1 and circ_0006896 (Fig. 3I, J).

Subsequently, to validate whether HDAC1 is the crucial functional target for circ_0006896, we selected chidamide, the commonly used HDAC1/2/3 inhibitor in the clinic, for conducting the in vivo and in vitro experiments. We first treated AML cells with chidamide and found that knockdown of circ_0006896 significantly enhanced the anti-leukemia effect of chidamide (Fig. 3K). These results were further validated in primary AML cells. The cell viability inhibition effect and apoptosis caused by chidamide was further enhanced with the knockdown of circ_0006896 (Fig. 3K, Supplementary Fig. 3G). Since our findings showed that circ_0006896 decreases AML cell sensitivity to IDA, we further treated AML cells with a combination of IDA and chidamide. The results showed that knockdown of circ_0006896 led to a much higher sensitivity of apoptosis upon IDA synergized with chidamide (Supplementary Fig. 3H). To further investigate the involvement of HDAC1 in the function of circ_0006896 in vivo, we intravenously injected sh-circ_0006896 or control Molm-13 cells into NOG mice, followed by treatment with 10 mg/kg chidamide or vehicle (DMSO + corn oil) by oral gavage every other day (Fig. 3L). We found that spleen size and weight in sh-circ_0006896 AML mice were significantly lower than that in control AML mice after chidamide treatment (Fig. 3M). Furthermore, flow cytometric results showed that the percentage of leukemia cells in bone marrow or spleen was significantly reduced in the sh-circ_0006896 AML mice after treatment with chidamide compared to that in control AML mice (Fig. 3N). Next, the survival of the animals was analyzed. As expected, sh-circ_0006896 AML mice had a significantly longer lifespan than control AML mice after treatment with chidamide (Fig. 3O), demonstrating that knockdown of circ_0006896 significantly promotes the AML therapeutic effect of chidamide in vivo. Together, these findings indicate that HDAC1 is a crucial functional target for circ_0006896 and knockdown of circ_0006896 significantly enhances the leukemia suppressive effects of chidamide in vitro and in vivo.

Inhibition of circ_0006896 promotes peroxidized lipids-induced ferroptosis, which is enhanced by HDAC inhibitor

Given that circ_0006896 is important for AML progression, we next performed RNA sequencing analysis in sh-circ_0006896 AML cells. We identified 466 differentially expressed genes ($|\log2\ (\text{Fold Change})| > 1.0$, P-value < 0.05) in circ_0006896-knockdown AML cells compared to control AML cells. Kyoto Encyclopedia of Genes and Genomes (KEGG) analysis of those differentially expressed genes indicated that arachidonic acid (AA) metabolism pathways are the top enriched pathways (Fig. 4A). And reactome analysis also showed that the genes related to AA metabolism were significantly enriched (Supplementary Fig. 4A). The gene set enrichment analysis (GSEA) analysis further showed that the ferroptosis and lipid oxidation pathways were significantly enriched in circ_0006896-knockdown AML cells (Fig. 4B). Gene Ontology (GO) analysis of those differentially expressed genes also showed that circ_0006896 was related to epigenetic or gene regulation pathways

(Supplementary Fig. 4B). These finding indicated that circ_0006896 is involved in signaling pathways related to peroxidized lipids-associated ferroptosis.

Therefore, we speculated that circ_0006896 might mitigate ferroptosis by preventing lipid peroxidation in AML cells. Consequently, we applied liquid chromatography-mass spectrometry (LC–MS) and ELISA to identify the major metabolites involved in the peroxidized lipids pathway. Our results revealed that 12S-hydroxyeicosatetraenoic acid (12S-HETE), docosahexaenoic acid, 15S-hydroxyeicosatetraenoic acid (15S-HETE), alpha-dimorphecolic acid (9S − HODE) and 5S-HETE were the most enriched metabolites in sh-circ_0006896 AML cells compared to control cells (Fig. 4 C, Supplementary Fig. 4C). Next, we further determined cellular ROS in circ_0006896-knockdown AML cells by flow cytometry. Our results showed that cellular ROS was increased in sh-circ_0006896 AML cells and significantly enhanced following chidamide treatment (Fig. 4D, Supplementary Fig. 4D). We further measured the lipid peroxidation level using BODIPY 581/591 C11. The results showed that the abundance of peroxidized lipids was significantly increased in sh-circ_0006896 AML cells, which could be further aggravated after chidamide treatment (Fig. 4E, Supplementary Fig. 4E). Moreover, knockdown of circ_0006896 significantly increased the level of MDA, a typical lipid peroxidation product, which also showed a noticeable enhancement in chidamide-treated AML cells (Fig. 4F, Supplementary Fig. 4F). Additionally, our results showed that the cell death caused by the downregulation of circ_0006896 was significantly mitigated by ferroptosis inhibitors ferrostain-1 and rosiglitazone (Fig. 4G, H). And, the application of ferrostain-1 and rosiglitazone significantly weakened the increased ROS and lipid peroxidation level induced by the knockdown of circ_0006896 (Fig. 4I, J, Supplementary Fig. 4G, H). In conclusion, these results suggest that circ_0006896 inhibition promotes ferroptosis synergistically with chidamide in AML cells.

To further explore how ferroptosis was regulated by circ_0006896 precisely, we further assessed the expression of genes related to ferroptosis or lipid peroxidation indicated in the RNA sequencing data. Results showed that the knockdown of circ_0006896 significantly increased the expression of AKR1C3, ALOX5, ACSL3, ACSL4 and LPCAT2 (Supplementary Fig. 4I). Considering the gene regulatory function of circ_0006896 in epigenetics via binding HDAC1 and the expression of these genes was significantly increased with the treatment of chidamide (Supplementary Fig. 4J), we further performed a ChIP assay to determine whether the promoters of these genes are epigenetically regulated by HDAC1 and circ_0006896. The results showed that knockdown of circ_0006896 significantly reduced the enrichment of HDAC1 in the promoter regions of these genes (Fig. 4K). Taken together, these data demonstrate that knockdown of circ_0006896 promotes the ferroptosis of AML cells by targeting HDAC1 and increasing the transcription of histone H3 acetylation related ferroptosis genes.

AML-derived exo-circ_0006896 impairs CD8$^+$ T cell cytotoxic function

Increasing evidence has revealed that AML-derived exosomes participate in TME via transferring non-coding RNAs, enabling AML cells to evade immune surveillance [27]. The KEGG analysis and GO enrichment analysis of our RNA-Seq data also suggested a close link between circ_0006896 and several immune regulatory pathways (Fig. 4A, Supplementary Fig. 5A). Immune cells, particularly CD8$^+$ T cells are crucial players in the TME [28, 29]. Therefore, we determined the apoptosis of CD8$^+$ T cells in bone marrow of primary AML patients and correlated it with the expression of circ_0006896. The results showed that the patients with higher circ_0006896 expression had a higher ratio of apoptosis in CD8$^+$ T cells ($n = 10$) (Fig. 5A, Supplementary Fig. 5B). We next evaluated the role of AML-derived exo-circ_0006896 in CD8$^+$ T cell anti-leukemia responses. First, we isolated exosomes from AML cells and incubated them with

(See figure on next page.)

Fig. 4 Downregulation of circ_0006896 synergized with chidamide induce cell death by modulating lipid peroxidation. **A** KEGG pathway enrichment analysis of the differently expressed genes potentially regulated by circ_0006896 in Molm-13 cells. **B** GSEA analysis of the differently expressed genes in circ_0006896-downregulated Molm-13 cells indicate the enrichment on ferroptosis and lipid oxidation pathways. **C** Metabolites of arachidonic acid enriched in circ_0006896 knockdown Molm-13 cells. **D**, **E** ROS and BODIPY C11 levels in circ_0006896-downregulated Molm-13 cells treated with chidamide. Statistical data were analyzed by One-Way ANOVA and multiple comparisons. **F** MDA in circ_0006896-downregulated Molm-13 cells treated with chidamide. **G**, **H** Cell death of circ_0006896 downregulated AML cells upon chidamide treatment and ferroptosis inhibitors. Antioxidant ferrostain-1 (2 μM, MCE, China) and ACSL4 inhibitor rosiglitazone (10 μM, MCE, China) were added 1 h before chidamide application. **I** ROS level in circ_0006896-downregulated Molm-13 cells treated with chidamide and ferroptosis inhibitors. **J** BODIPY C11 level of circ_0006896-downregulated Molm-13 cells treated with chidamide and ferroptosis inhibitors. **K** ChIP assay determined the enrichment of HDAC1 in the promoter regions of ferroptosis-associated genes and its regulation by circ_0006896. Statistical data in F and H–K were analyzed by Student's t-test. Statistical data were presented in mean ± SD, $^{**}P \le 0.01$, $^{***}P \le 0.001$, $^{****}P \le 0.0001$ and ns indicates $P > 0.05$

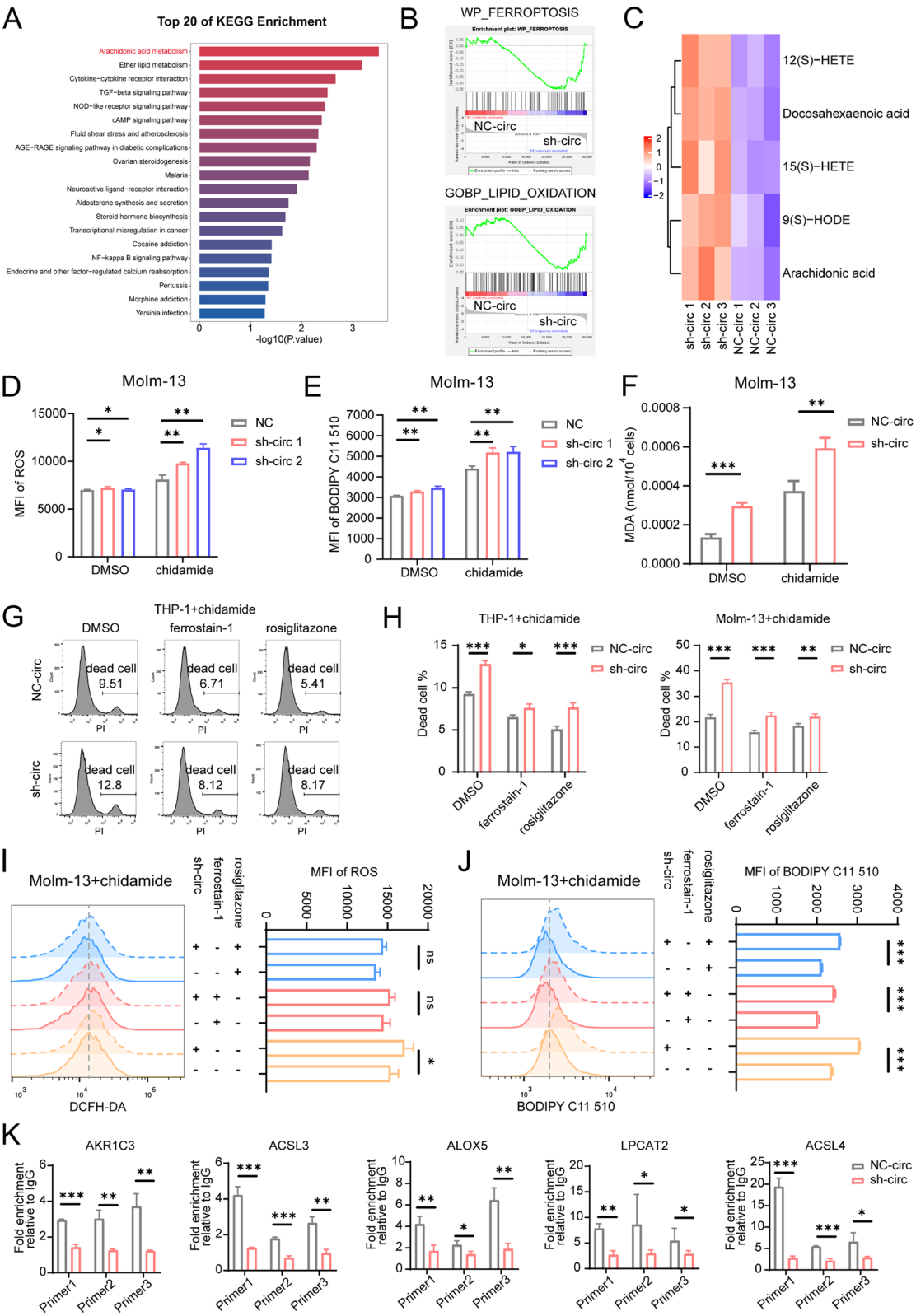

Fig. 4 (See legend on previous page.)

activated $CD8^+$ T cells (Fig. 5B). The results showed that AML-derived exosomes were apparently absorbed by $CD8^+$ T cells (Fig. 5C). The RT-qPCR results revealed that circ_0006896 was significantly up-regulated in $CD8^+$ T cells after treatment with AML exosomes compared to PBS control, whereas this upregulation was weakened with sh-circ_0006896 AML exosomes (Supplementary Fig. 5C). To further evaluate the effect of exo-circ_0006896 on tumor-specific cytotoxic T lymphocytes (CTLs), we used AML cell lysates to sensitize dendritic cells, which were then co-cultured with $CD8^+$ T cells in the presence of sh-circ_0006896 AML-derived exosomes or control AML exosomes (Fig. 5D). We further assessed the cytotoxic function of T cells using flow cytometry. Our results demonstrated a noteworthy increase in TNF-α and granzyme B levels in $CD8^+$ T cells after treatment with sh-circ_0006896 exosomes (Fig. 5E), indicating enhanced $CD8^+$ T cell function induced by sh-circ_0006896 AML exosomes. To assess whether these findings could be extended to primary AML cells, we used exosomes from 3 patients with higher circ_0006896 expressions and 3 patients with lower circ_0006896 expressions (Fold change > 2) to treat AML-specific $CD8^+$ T cells. The same results of increased IFN-γ and granzyme B levels in $CD8^+$ T cells were demonstrated in our experiments (Fig. 5F). Moreover, treatment of $CD8^+$ T cells with higher circ_0006896 exosomes induced obvious apoptosis in $CD8^+$ T cells, whereas the treatment with lower circ_0006896 exosomes significantly reduced the apoptosis caused by activation and exosomes (Fig. 5G). To further evaluate the cytotoxic function of T cells incubated with AML exosomes, we co-cultured them with primary AML cells or Molm-13 cells, and then assessed the apoptosis of AML cells using flow cytometry. Results showed that NC-circ exosomes or high circ_0006896 exosomes treated $CD8^+$ T cells induced significant apoptosis in Molm-13 cells and primary AML cells, and treatment with sh-circ_0006896 AML exosomes or low circ_0006896 exosomes further increased the cytotoxic function of $CD8^+$ T cells, indicating that exosomes with higher expression of circ_0006896 could impair the cytotoxicity of AML-specific $CD8^+$ T cells (Fig. 5H, I).

To further investigate the role of endogenous circ_0006896 in $CD8^+$ T cells, we transfected $CD8^+$ T cells with sh-circ_0006896. Similar results were observed that knockdown of circ_0006896 increased the proportions of IFN-γ and TNF-α in $CD8^+$ T cells (Fig. 5J), and the results also demonstrated that inhibition of circ_0006896 significantly reduced activation-induced apoptosis of $CD8^+$ T cell (Fig. 5K). Collectively, all these data suggest that inhibition of AML-derived exo-circ_0006896 suppresses the immune evasion of AML cells by enhancing $CD8^+$ T cells anti-leukemia function.

Inhibition of circ_0006896 and HDAC1 synergistically suppresses AML progression by enhancing $CD8^+$ T cell cytotoxic function

We next sought to understand the mechanism by which AML-derived exo-circ_0006896 impairs $CD8^+$ T anti-leukemia activity. It has been reported that inhibiting HDACs or increasing histone acetylation could enhance the antitumor activities of CTLs [30, 31]. To test whether circ_0006896 contributes to the cytotoxicity of AML-antigen-activated CTLs in a manner related to HDAC1 activity, we performed an RNA pull-down assay with a 3'-biotinylated circ_0006896 on CTLs protein lysates, followed by SDS-PAGE. After silver staining, we observed a sense-specific band around 55 kDa (Supplementary Fig. 5D, red frame). We then validated the interaction between circ_0006896 and HDAC1 using western blot in CTLs (Fig. 6A). As expected, RIP assay for HDAC1 also showed strong enrichment of circ_0006896 in CTL protein lysates (Fig. 6B). Importantly, sh-circ_0006896 exosome treatment resulted in significantly higher H3K9 and H3K27 acetylation level compared to control AML exosomes (Fig. 6C).

As HDAC1 regulates multiple gene expression programs by influencing histone acetylation-regulated transcription, we questioned whether AML-derived exo-circ_0006896 regulates $CD8^+$ T cell anti-leukemia

(See figure on next page.)

Fig. 5 AML-derived exosomal circ_0006896 restricts $CD8^+$ T cell cytotoxic function. **A** Apoptosis ratio of $CD8^+$ T cells in AML patients' bone marrow. Statistical data were represented in median with range and analyzed with Mann–Whitney U tests. **B** Schematic diagram illustrating the exosomes treatment on $CD8^+$ T cells. **C** Representative image showing PKH67-labeled AML-derived exosomes uptake by $CD8^+$ T cells (Scale bar = 5 μm). **D** Schematic illustration of induction of AML-antigen-activated $CD8^+$ T cells and the treatment of exosomes. **E** Function of $CD8^+$ T cells after treatment with NC-circ or sh-circ exosomes. **F** Function of $CD8^+$ T cells after treated with circ_0006896 high-expressing or low-expressing exosomes from AML patients. **G** Apoptosis of $CD8^+$ T cells after being treated with circ_0006896 high-expressing or low-expressing exosomes from AML patients. **H** Apoptosis of primary AML cells caused by $CD8^+$ T cells treated with circ_0006896 high-expressing or low-expressing exosomes. **I** Apoptosis of Molm-13 cells induced by $CD8^+$ T cells treated with NC-circ or sh-circ exosomes. **J** Function of endogenous circ_0006896-downregulated $CD8^+$ T cells. **K** Apoptosis of CD8.$^+$ T cells induced by endogenous circ_0006896 knockdowns. Statistical data in F, G, H were presented in mean ± SD and analyzed by Student's t-test. Statistical data in E, I, J, K were analyzed by Paired Student's t-test. *$P \le 0.05$, **$P \le 0.01$, ***$P \le 0.001$, ****$P \le 0.0001$ and ns indicates $P > 0.05$

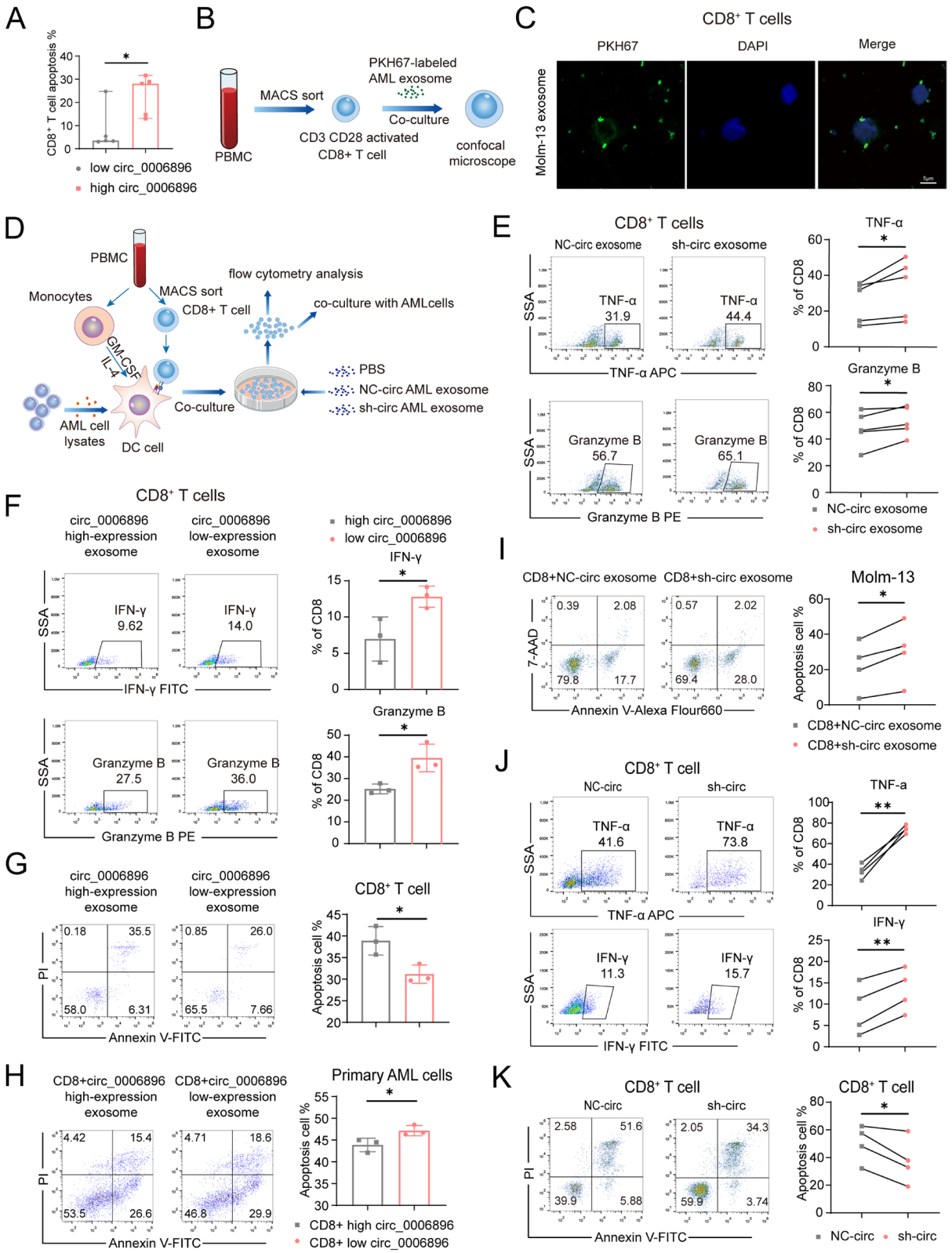

Fig. 5 (See legend on previous page.)

activity via HDAC1-mediated transcriptional modulation. Therefore, we further assessed whether the known transcription factors and functional molecules for $CD8^+$ T cell function were regulated by HDAC1. Our results showed that knockdown of circ_0006896 significantly increased the expression of T-bet, Blimp1, LEF1, IFN-γ, Granzyme B and TNF-α (Supplementary Fig. 5E). We then co-cultured $CD8^+$ T cells with sh-circ_0006896 AML exosomes or control AML exosomes. Results showed that LEF1 expression levels were significantly higher in sh-circ_0006896 exosome-treated $CD8^+$ T cells than in those treated with control AML exosomes (Supplementary Fig. 5F). Moreover, we also performed a ChIP assay to determine whether the LEF1 promoter is epigenetically regulated by HDAC1 and circ_0006896. Our results showed that knockdown of circ_0006896 significantly decreased the enrichment of HDAC1 in LEF1 promoter (Fig. 6D). Together, these data demonstrate that knockdown of circ_0006896 restores $CD8^+$ T cell function by targeting HDAC1 and enhancing H3 acetylation-related gene transcriptional activity.

Since exo-circ_0006896 inhibits the LEF1 expression via interacting with HDAC1 in $CD8^+$ T cells, we further investigated their effects on $CD8^+$ T cell anti-leukemia activity. AML-specific $CD8^+$ T cells stimulated with AML-antigen-pulsed DCs were treated with chidamide in the presence of sh-circ_0006896 exosomes or control exosomes. As expected, treatment with chidamide induced a significant reduction in $CD8^+$ T cell apoptosis. Moreover, sh-circ_0006896 exosomes significantly enhanced chidamide effect, resulting in a lower apoptotic percentage of $CD8^+$ T cells compared to the control exosomes (Supplementary Fig. 5G). We also observed a higher level of cytotoxic functional molecules, TNF-α and granzyme B, in sh-circ_0006896 exosome-treated $CD8^+$ T cells after chidamide treatment (Fig. 6E), indicating that circ_0006896 inhibition restores $CD8^+$ T cell function synergistically with chidamide. The same synergistic enhancement effects were observed when we treated the AML-specific $CD8^+$ T cells with patients derived circ_0006896 low-expressing exosomes and chidamide (Fig. 6F).

Furthermore, we investigated whether circ_0006896 downregulation in the AML-exosomes could alleviate transferred T cell dysfunction and improve HDAC1 inhibitor effects in xenotransplantation AML mouse model. Molm-13 cells were intravenously injected into NOG mice to establish a xenotransplantation AML mouse model. After 5 days, AML-specific $CD8^+$ T cells cultured with sh-circ_0006896 exosomes or control exosomes were intravenously injected into mice, followed by treatment with 10 mg/kg chidamide (Fig. 6G). We first investigated the fate of transferred CTLs in peripheral blood. Flow cytometry results showed that the percentage of $CD8^+$ T cells was remarkably higher in the mice treated with exo-sh-circ_0006896 CTLs and further increased after treatment with chidamide (Supplementary Fig. 5H, J). We also found that treatment with exo-sh-circ_0006896 CTLs significantly reduced the spleen size and weight in AML mice, and this reduction was further enhanced after chidamide treatment (Fig. 6H). Flow cytometry results demonstrated that adoptive transfer of CTLs cultured with sh-circ_0006896 exosomes significantly reduced the percentage of leukemia cells in peripheral blood, bone marrow and spleen, thereby effectively inhibiting AML progression. Furthermore, after treatment with chidamide, the percentage of leukemia cells in peripheral blood, bone marrow and spleen further significantly decreased in mice treated with exo-sh-circ_0006896 CTLs compared to control exosomes (Fig. 6I, Supplementary Fig. 5K). Moreover, the cytotoxic function of CTLs was much more enhanced in sh-circ_0006896 exosome-treated mice compared to control exosome-treated mice, and this effect was further amplified by chidamide treatment (Fig. 6J-M, Supplementary Fig. 5I). The survival time of these mice followed the same trend: CTLs cultured with sh-circ_0006896 exosomes prolonged mouse survival compared to control exosomes, and this superiority was further amplified by chidamide treatment (Fig. 6N). Collectively,

(See figure on next page.)

Fig. 6 Inhibition of circ_0006896 and HDAC1 synergistically suppresses AML progression by enhancing $CD8^+$ T cell cytotoxic function. **A** Western blot of HDAC1 in circ_0006896 RNA pull-down proteins in $CD8^+$ T cells. **B** Circ_0006896 PCR analysis of RIP assay using HDAC1 antibody performed in $CD8^+$ T cells. Statistical data were analyzed by Student's t-test. **C** Western blot of Ac-H3k27 and Ac-K3K9 in $CD8^+$ T cells treated with NC-circ and sh-circ exosomes. **D** ChIP assay determining HDAC1 enrichment at the LEF1 promoter region and its regulation by circ_0006896. Statistical data were analyzed by Student's t-test. **E** Function of $CD8^+$ T cells treated with AML cells derived exosomes and chidamide. Statistical data were analyzed by paired Student's t-test. **F** Function of $CD8^+$ T cells treated with AML patients derived exosomes and chidamide. Statistical data were analyzed by Student's t-test. **G** Schematic diagram illustrating the preparation and adoptive transfer of exosome-treated AML-antigen-activated $CD8^+$ T cells and the treatment of chidamide. **H** Representative image and spleen weight of mice. **I** Leukemic burden of Molm-13 cells in the bone marrow and spleen ($n=4$). **J-M** Function of CD8.$^+$ T cells evaluated by flow cytometry. **N** Survival analysis of the mice treated as indicated ($n=4$). Statistical data in H, I, K, M were analyzed by Two-Way ANOVA and multiple comparisons. Statistical data presented in mean ± SD, $^*P \le 0.05$, $^{**}P \le 0.01$, $^{***}P \le 0.001$, $^{****}P \le 0.0001$ and ns indicates $P > 0.05$

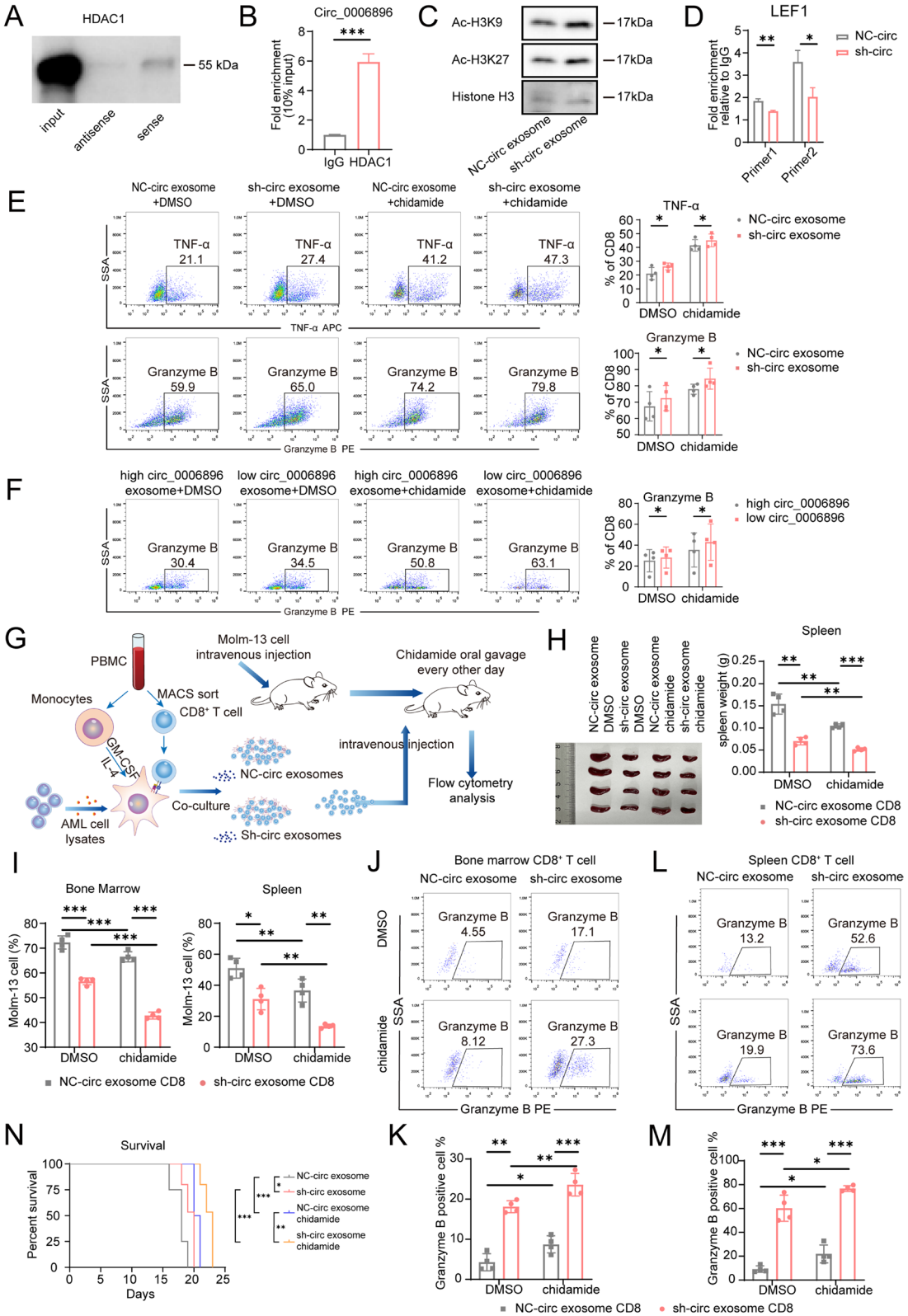

Fig. 6 (See legend on previous page.)

these findings suggest that synergistic inhibition of circ_0006896 and HDAC1 in the transferred AML-reactive CTLs overcomes AML immune evasion by enhancing CD8$^+$ T cell activity, thus improving the therapeutic effects of adoptive T cell therapy for AML.

Discussion

Despite exosomes derived from AML have been shown to promote the progression of AML by regulating the bone marrow microenvironment, whereas the molecular mechanisms involved are still largely unknown. This study revealed that circ_0006896 is highly expressed in the leukemia cells and exosomes of AML patients. In addition, exosomal circ_0006896 is a more sensitive biomarker correlated with the poor prognosis of AML. Elevated expression of circ_0006896 in AML cells and AML exosomes promotes AML progression in vivo and in vitro. Inhibition of circ_0006896 enhances apoptosis and ferroptosis in AML cells during chemotherapy by acting as a molecular scaffold for HDAC1, promoting the acetylation of histone 3 and sustaining lipid peroxidation-induced ferroptosis. Furthermore, AML exo-circ_0006896 impairs CD8$^+$ T cell cytotoxicity by interacting with HDAC1, reducing the transcription of key transcription factors of T cells, thus promoting AML immune evasion (Fig. 7). Our findings uncover a new role of circ_0006896 in AML chemotherapy sensitivity and immune evasion by altering HDAC1-mediated epigenetic reprogramming, proposing circ_0006896 as a potential therapeutic target for AML.

According to our previous results, circRNAs exhibit an overall low expression trend in AML, which may contribute to the quiescence and inhibited differentiation of LSCs. For the first time, we found that the circRNA expression pattern in exosomes, based on sample clustering and principal component analysis, differed more significantly between AML patients and healthy controls than lncRNAs or mRNAs. This suggests that circRNAs may play a more stable role in exosomes. Our study revealed an AML progression pattern driven by

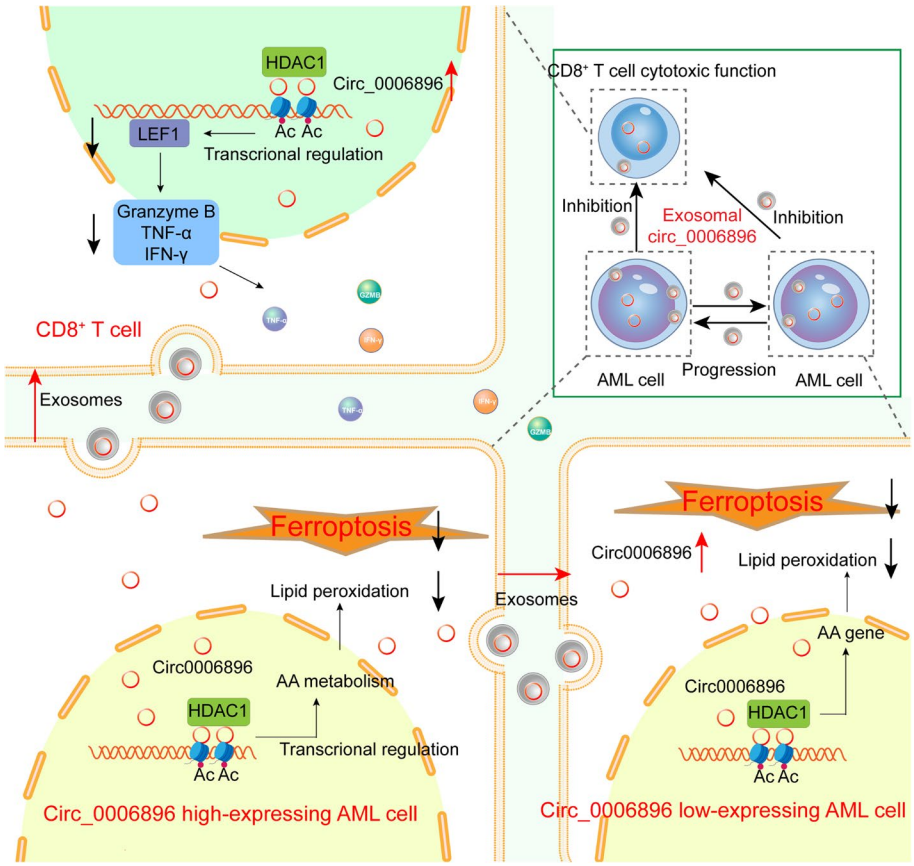

Fig. 7 Schematic depiction of how exosomal circ_0006896 promotes AML progression and immune evasion. High expression of circ_0006896 promotes AML cell progression by inhibiting lipid peroxidation-induced ferroptosis via binding HDAC1. Additionally, exosomal circ_0006896 absorbed by CD8$^+$ T cells induces the dysfunction of T cells by modulating HDAC1 and impairing the transcription of LEF1 and related functional molecules

the autocrine and paracrine signaling of exosomal circRNAs. Endogenous and exosomal circ_0006896 both promoted the progression of AML cells. At the same time, the exosomal circ_0006896 impaired the function of CTLs and promoted the immune evasion of AML cells. Therefore, our study confirms that some highly expressed circRNAs have another significant oncogenic effect in AML.

The oncogenesis and progression of AML are profoundly influenced by epigenetic regulation. Targeting epigenetic regulators of histone H3 acetylation could reverse the aberrant transcription of oncogene and improve the outcomes in AML patients [32–34]. HDACs, by regulating the deacetylation of histones, decrease the affinity between DNA and transcription factors and lead to the inhibition of antitumor gene transcription. General HDAC inhibitors have been reported to exhibit significant antitumor activity combined with other therapeutics in AML [35, 36]. However, little is known about how the HDAC1 protein is regulated and how it functions. Our results indicate that upregulated circ_0006896 physically interacts with HDAC1, acting as a scaffold to facilitate the deacetylation of histone H3, thus reprogramming epigenetic regulation in AML cells. Exosomal autocrine signaling from AML cells could significantly reshape the AML progression and drug resistance. Knockdown of circ_0006896, in synergy with chidamide, significantly inhibits the activity of HDAC1 and increases the sensitivity of AML cells to IDA, implying the possibility of circ_0006896 as a potential target for combined chemotherapy.

Arachidonic acid plays a broad role in inflammatory response and cancer development [37]. On the one hand, AA can be metabolized into prostaglandins (PGs) by cyclooxygenase (COX) and into leukotrienes (LTs) by lipoxygenase (LOX), among which, prostaglandin E2 (PGE2) promotes inflammation and cancer progression notably [38, 39]. On the other hand, arachidonic acid metabolism may act as a signal of ferroptosis, as it is catalyzed in the linear peroxidation of polyunsaturated fatty acid (PUFA), resulting in the generation of hydroperoxides molecules [40, 41]. Recent studies have demonstrated that lipid peroxidation, catalyzed by lipoxygenases, primarily ALOX5, ALOX12 and ALOX15, plays a crucial role in triggering ferroptosis [42–44]. Interestingly, downregulation of circ-006896 enhanced arachidonic acid metabolism, shifted its metabolite profile toward LOX-derived lipid peroxidation and resulted in increased accumulation of hydrogen peroxide downstream products rather than PGs and LTs. And knockdown of circ_006896 also induced the up-regulation of genes involved in ferroptosis pathway, ultimately leading to lipid peroxide-mediated ferroptosis.

Impaired antitumor immunity, characterized by decreased frequency of functioning $CD8^+$ T cells and high expression of immune exhaustion markers, has been observed in peripheral blood and bone marrow of AML patients [45]. Overcoming the immune escape of AML cells may be the key to the treatment of relapsed/refractory AML. It has been reported that cancer cell-derived exosomal circTRPS1 and circCCAR1 promoted $CD8^+$ T cell exhaustion in bladder cancer and hepatocellular carcinoma[46, 47]. Exosomal circRNAs can also act as vaccine adjuvants, increasing the efficacy of the vaccine and inducing antigen-specific T cell activation [48, 49]. These data denote the possibility of circRNAs in impairing $CD8^+$ T cell immune response, but few studies have explored the mechanism by which AML-derived exosomes regulate the epigenetic reprogramming in $CD8^+$ T cells. Here, we found that exosomal circ_0006896 inhibits AML-specific $CD8^+$ T cells' function by interacting with HDAC1, and further reducing LEF1 transcription via diminishing histone 3 acetylation at the LEF1 promoter region. Previous studies have shown that the application of HDAC inhibitors could enhance the infiltration and antitumor activities of CTLs, improve memory phenotype maintenance and impair CAR-T cell exhaustion by increasing histone acetylation [50–53]. In conclusion, we identified that inhibition of exosomal circ_006896 in T cells enhances their antitumor function in adoptive cell-transfer therapy, particularly when synergized with HDAC1 inhibitor. Our data provide a demonstration that exosomal circRNAs may play important roles in the dysfunction and limited persistence of $CD8^+$ T cells in adoptive transferring therapy. Targeting exosomal circ_006896 and HDAC1 may be an exploitable therapeutic approach for AML patients.

Conclusion

Our study demonstrates that AML-derived exosomal circ_006896 promotes AML progression by acting as a molecular scaffold for HDAC1 and impairing the cytotoxic function of $CD8^+$ T cells. We broaden the cognizance of circRNAs in promoting tumor progression and reshaping the bone marrow immune microenvironment in AML.

Supplementary Information

The online version contains supplementary material available at https://doi.org/10.1186/s12943-024-02203-8.

Supplementary Material 1.

Acknowledgements

The authors thank all participating patients, without whom continuous improvement in clinical care and growing scientific insights would not be

possible. The authors acknowledge all contributing physicians, study nurses, and laboratories for their support in the trials.

Authors' contributions
Professor D.X.M. designed and funded the study. C.C. and X.Y.Y. performed this research. H.X.J. and H.Y.W. assisted with this research. Y.H.W., Z.T.J and X.D.G. analyzed the data. A.M.Z., N.H., H.L.Z and W.C.L. revised the manuscript accordingly. C.C. and X.Y.Y. wrote the manuscript.

Funding
This work was supported by grants from the National Natural Science Foundation of China (No. 82370173, 32241005).

Data availability
Transcriptome sequencing data that support the findings of this study can be found in the online repositories of GEO (GSE285301).

Declarations

Ethics approval and consent to participate
The trials were approved by the respective ethics committees and were conducted in accordance with the Declaration of Helsinki (KYLL-202204–059). All patients provided written informed consent, including the analysis of data. The studies were continuously monitored using clinical and medical monitoring. Animal studies were approved by the ethics committee on animal experiment, Qilu hospital of Shandong university (DWLL-2023–057).

Consent for publication
Not applicable.

Competing interests
The authors declare no competing interests.

Received: 9 October 2024 Accepted: 18 December 2024
Published online: 06 January 2025

References

1. Foreman KJ, Marquez N, Dolgert A, Fukutaki K, Fullman N, McGaughey M, Pletcher MA, Smith AE, Tang K, Yuan CW, et al. Forecasting life expectancy, years of life lost, and all-cause and cause-specific mortality for 250 causes of death: reference and alternative scenarios for 2016–40 for 195 countries and territories. Lancet. 2018;392(10159):2052–90.
2. Estey E, Dohner H. Acute myeloid leukaemia. Lancet. 2006;368(9550):1894–907.
3. Dombret H, Gardin C. An update of current treatments for adult acute myeloid leukemia. Blood. 2016;127(1):53–61.
4. Dohner H, Wei AH, Appelbaum FR, Craddock C, DiNardo CD, Dombret H, Ebert BL, Fenaux P, Godley LA, Hasserjian RP, et al. Diagnosis and management of AML in adults: 2022 recommendations from an international expert panel on behalf of the ELN. Blood. 2022;140(12):1345–77.
5. Bhansali RS, Pratz KW, Lai C. Recent advances in targeted therapies in acute myeloid leukemia. J Hematol Oncol. 2023;16(1):29.
6. Mendes M, Monteiro AC, Neto E, Barrias CC, Sobrinho-Simoes MA, Duarte D, Caires HR. Transforming the Niche: The Emerging Role of Extracellular Vesicles in Acute Myeloid Leukaemia Progression. Int J Mol Sci. 2024;25(8):4430.
7. Amin AH, Sharifi LMA, Kakhharov AJ, Opulencia MJC, Alsaikhan F, Bokov DO, Majdi HS, Jawad MA, Hammid AT, Shalaby MN, et al. Role of Acute Myeloid Leukemia (AML) Derived exosomes in tumor progression and survival. Biomed Pharmacother. 2022;150.
8. Chen Y, Wen J, Li Q, Peng D, Liao C, Ma X, Wang M, Niu J, Wang D, Li Y, et al. RAB27B-regulated exosomes mediate LSC maintenance via resistance to senescence and crosstalk with the microenvironment. Leukemia. 2024;38(2):266–80.
9. Zhang L, Zhao Q, Cang H, Wang Z, Hu X, Pan R, Yang Y, Chen Y. Acute Myeloid Leukemia Cells Educate Mesenchymal Stromal Cells toward an Adipogenic Differentiation Propensity with Leukemia Promotion Capabilities. Adv Sci (Weinh). 2022;9(16):2105811.
10. Du A, Yang Q, Sun X, Zhao Q. Exosomal circRNA-001264 promotes AML immunosuppression through induction of M2-like macrophages and PD-L1 overexpression. Int Immunopharmacol. 2023;124(Pt A):110868.
11. Otmani K, Rouas R, Lagneaux L, Krayem M, Duvillier H, Berehab M, Lewalle P. Acute myeloid leukemia-derived exosomes deliver miR-24-3p to hinder the T-cell immune response through DENN/MADD targeting in the NF-kappaB signaling pathways. Cell Commun Signal. 2023;21(1):253.
12. Wang J, Pan J, Huang S, Li F, Huang J, Li X, Ling Q, Ye W, Wang Y, Yu W, et al. Development and validation of a novel circular RNA as an independent prognostic factor in acute myeloid leukemia. BMC Med. 2021;19(1):28.
13. Sun H, Xie Y, Wu X, Hu W, Chen X, Wu K, Wang H, Zhao S, Shi Q, Wang X, et al. circRNAs as prognostic markers in pediatric acute myeloid leukemia. Cancer Lett. 2024;591:216880.
14. Liu X, Liu X, Cai M, Luo A, He Y, Liu S, Zhang X, Yang X, Xu L, Jiang H. CircRNF220, not its linear cognate gene RNF220, regulates cell growth and is associated with relapse in pediatric acute myeloid leukemia. Mol Cancer. 2021;20(1):139.
15. Lin L, Wang Y, Bian S, Sun L, Guo Z, Kong D, Zhao L, Guo D, Li Q, Wu M, et al. A circular RNA derived from PLXNB2 as a valuable predictor of the prognosis of patients with acute myeloid leukaemia. J Transl Med. 2021;19(1):123.
16. Yang X, Han F, Hu X, Li G, Wu H, Can C, Wei Y, Liu J, Wang R, Jia W, et al. EIF4A3-induced Circ_0001187 facilitates AML suppression through promoting ubiquitin-proteasomal degradation of METTL3 and decreasing m6A modification level mediated by miR-499a-5p/RNF113A pathway. Biomark Res. 2023;11(1):59.
17. Yang X, Liu J, Liu W, Wu H, Wei Y, Guo X, Jia H, Can C, Wang D, Hu X, et al. circFAM193B interaction with PRMT6 regulates AML leukemia stem cells chemoresistance through altering the oxidative metabolism and lipid peroxidation. Leukemia. 2024;38(5):1057–71.
18. Zhao A, Zhou H, Yang J, Li M, Niu T. Epigenetic regulation in hematopoiesis and its implications in the targeted therapy of hematologic malignancies. Signal Transduct Target Ther. 2023;8(1):71.
19. Yamagishi M, Kuze Y, Kobayashi S, Nakashima M, Morishima S, Kawamata T, Makiyama J, Suzuki K, Seki M, Abe K, et al. Mechanisms of action and resistance in histone methylation-targeted therapy. Nature. 2024;627(8002):221–8.
20. Park SY, Kim JS. A short guide to histone deacetylases including recent progress on class II enzymes. Exp Mol Med. 2020;52(2):204–12.
21. Wang H, Liu YC, Zhu CY, Yan F, Wang MZ, Chen XS, Wang XK, Pang BX, Li YH, Liu DH, et al. Chidamide increases the sensitivity of refractory or relapsed acute myeloid leukemia cells to anthracyclines via regulation of the HDAC3 -AKT-P21-CDK2 signaling pathway. J Exp Clin Cancer Res. 2020;39(1):278.
22. Lai QY, He YZ, Peng XW, Zhou X, Liang D, Wang L. Histone deacetylase 1 induced by neddylation inhibition contributes to drug resistance in acute myelogenous leukemia. Cell Commun Signal. 2019;17(1):86.
23. Dai B, Wang F, Wang Y, Zhu J, Li Y, Zhang T, Zhao L, Wang L, Gao W, Li J, et al. Targeting HDAC3 to overcome the resistance to ATRA or arsenic in acute promyelocytic leukemia through ubiquitination and degradation of PML-RARalpha. Cell Death Differ. 2023;30(5):1320–33.
24. Zhou C, Li W, Liang Z, Wu X, Cheng S, Peng J, Zeng K, Li W, Lan P, Yang X, et al. Mutant KRAS-activated circATXN7 fosters tumor immunoescape by sensitizing tumor-specific T cells to activation-induced cell death. Nat Commun. 2024;15(1):499.
25. Paskeh MDA, Entezari M, Mirzaei S, Zabolian A, Saleki H, Naghdi MJ, Sabet S, Khoshbakht MA, Hashemi M, Hushmandi K, et al. Emerging role of exosomes in cancer progression and tumor microenvironment remodeling. J Hematol Oncol. 2022;15(1):83.
26. Xu Z, Chen Y, Ma L, Chen Y, Liu J, Guo Y, Yu T, Zhang L, Zhu L, Shu Y. Role of exosomal non-coding RNAs from tumor cells and tumor-associated macrophages in the tumor microenvironment. Mol Ther. 2022;30(10):3133–54.
27. Melo SA, Sugimoto H, O'Connell JT, Kato N, Villanueva A, Vidal A, Qiu L, Vitkin E, Perelman LT, Melo CA, et al. Cancer exosomes perform cell-independent microRNA biogenesis and promote tumorigenesis. Cancer Cell. 2014;26(5):707–21.
28. Bejarano L, Jordao MJC, Joyce JA. Therapeutic Targeting of the Tumor Microenvironment. Cancer Discov. 2021;11(4):933–59.

29. Hiam-Galvez KJ, Allen BM, Spitzer MH. Systemic immunity in cancer. Nat Rev Cancer. 2021;21(6):345–59.
30. Liu G, Barczak W, Lee LN, Shrestha A, Provine NM, Albayrak G, Zhu H, Hutchings C, Klenerman P, La Thangue NB. The HDAC inhibitor zabadinostat is a systemic regulator of adaptive immunity. Commun Biol. 2023;6(1):102.
31. Que Y, Zhang XL, Liu ZX, Zhao JJ, Pan QZ, Wen XZ, Xiao W, Xu BS, Hong DC, Guo TH, et al. Frequent amplification of HDAC genes and efficacy of HDAC inhibitor chidamide and PD-1 blockade combination in soft tissue sarcoma. J Immunother Cancer. 2021;9(2):e001696.
32. Gambacorta V, Gnani D, Vago L, Di Micco R. Epigenetic Therapies for Acute Myeloid Leukemia and Their Immune-Related Effects. Front Cell Dev Biol. 2019;7:207.
33. Issa GC, Aldoss I, DiPersio J, Cuglievan B, Stone R, Arellano M, Thirman MJ, Patel MR, Dickens DS, Shenoy S, et al. The menin inhibitor revumenib in KMT2A-rearranged or NPM1-mutant leukaemia. Nature. 2023;615(7954):920–4.
34. Palau A, Segerberg F, Lidschreiber M, Lidschreiber K, Naughton AJ, Needhamsen M, Jung LA, Jagodic M, Cramer P, Lehmann S, et al. Perturbed epigenetic transcriptional regulation in AML with IDH mutations causes increased susceptibility to NK cells. Leukemia. 2023;37(9):1830–41.
35. Ye J, Zha J, Shi Y, Li Y, Yuan D, Chen Q, Lin F, Fang Z, Yu Y, Dai Y, et al. Co-inhibition of HDAC and MLL-menin interaction targets MLL-rearranged acute myeloid leukemia cells via disruption of DNA damage checkpoint and DNA repair. Clin Epigenetics. 2019;11(1):137.
36. Zhao H, Jiang Y, Lin F, Zhong M, Tan J, Zhou Y, Liu L, Li G, Deng M, Xu B. Chidamide and apatinib are therapeutically synergistic in acute myeloid leukemia stem and progenitor cells. Exp Hematol Oncol. 2022;11(1):29.
37. Bae S, Kim MK, Kim HS, Moon YA. Arachidonic acid induces ER stress and apoptosis in HT-29 human colon cancer cells. Anim Cells Syst (Seoul). 2020;24(5):260–6.
38. Yang H, Rothenberger E, Zhao T, Fan W, Kelly A, Attaya A, Fan D, Panigrahy D, Deng J. Regulation of inflammation in cancer by dietary eicosanoids. Pharmacol Ther. 2023;248:108455.
39. Veglia F, Tyurin VA, Blasi M, De Leo A, Kossenkov AV, Donthireddy L, To TKJ, Schug Z, Basu S, Wang F, et al. Fatty acid transport protein 2 reprograms neutrophils in cancer. Nature. 2019;569(7754):73–8.
40. Cai W, Liu L, Shi X, Liu Y, Wang J, Fang X, Chen Z, Ai D, Zhu Y, Zhang X. Alox15/15-HpETE Aggravates Myocardial Ischemia-Reperfusion Injury by Promoting Cardiomyocyte Ferroptosis. Circulation. 2023;147(19):1444–60.
41. Cantonero C, Sanchez-Collado J, Lopez JJ, Salido GM, Rosado JA, Redondo PC. Arachidonic Acid Attenuates Cell Proliferation, Migration and Viability by a Mechanism Independent on Calcium Entry. Int J Mol Sci. 2020;21(9):3315.
42. Liu T, Xu X, Li J, Bai M, Zhu W, Liu Y, Liu S, Zhao Z, Li T, Jiang N, et al. ALOX5 deficiency contributes to bladder cancer progression by mediating ferroptosis escape. Cell Death Dis. 2023;14(12):800.
43. Chu B, Kon N, Chen D, Li T, Liu T, Jiang L, Song S, Tavana O, Gu W. ALOX12 is required for p53-mediated tumour suppression through a distinct ferroptosis pathway. Nat Cell Biol. 2019;21(5):579–91.
44. Wang D, Wang F, Zhang H, Chen P, Yang M. Circadian clock protein Bmal1 accelerates acute myeloid leukemia by inhibiting ferroptosis through the EBF3/ALOX15 axis. Cancer Sci. 2023;114(8):3446–60.
45. Romine KA, MacPherson K, Cho HJ, Kosaka Y, Flynn PA, Byrd KH, Coy JL, Newman MT, Pandita R, Loo CP, et al. BET inhibitors rescue anti-PD1 resistance by enhancing TCF7 accessibility in leukemia-derived terminally exhausted CD8(+) T cells. Leukemia. 2023;37(3):580–92.
46. Yang C, Wu S, Mou Z, Zhou Q, Dai X, Ou Y, Chen X, Chen Y, Xu C, Hu Y, et al. Exosome-derived circTRPS1 promotes malignant phenotype and CD8+ T cell exhaustion in bladder cancer microenvironments. Mol Ther. 2022;30(3):1054–70.
47. Hu Z, Chen G, Zhao Y, Gao H, Li L, Yin Y, Jiang J, Wang L, Mang Y, Gao Y, et al. Exosome-derived circCCAR1 promotes CD8 + T-cell dysfunction and anti-PD1 resistance in hepatocellular carcinoma. Mol Cancer. 2023;22(1):55.
48. Ren Y, Manoharan T, Liu B, Cheng CZM, En Siew B, Cheong WK, Lee KY, Tan IJ, Lieske B, Tan KK, et al. Circular RNA as a source of neoantigens for cancer vaccines. J Immunother Cancer. 2024;12(3):e008402.
49. Huang D, Zhu X, Ye S, Zhang J, Liao J, Zhang N, Zeng X, Wang J, Yang B, Zhang Y, et al. Tumour circular RNAs elicit anti-tumour immunity by encoding cryptic peptides. Nature. 2024;625(7995):593–602.
50. Wang X, Waschke BC, Woolaver RA, Chen SMY, Chen Z, Wang JH. HDAC inhibitors overcome immunotherapy resistance in B-cell lymphoma. Protein Cell. 2020;11(7):472–82.
51. Lin Y, Jing X, Chen Z, Pan X, Xu D, Yu X, Zhong F, Zhao L, Yang C, Wang B, et al. Histone deacetylase-mediated tumor microenvironment characteristics and synergistic immunotherapy in gastric cancer. Theranostics. 2023;13(13):4574–600.
52. Wen T, Sun G, Jiang W, He X, Shi Y, Ma F, Liu P. Histone deacetylases inhibitor chidamide synergizes with humanized PD1 antibody to enhance T-cell chemokine expression and augment Ifn-gamma response in NK-T cell lymphoma. EBioMedicine. 2023;87:104420.
53. Zhu M, Han Y, Gu T, Wang R, Si X, Kong D, Zhao P, Wang X, Li J, Zhai X, et al. Class I HDAC inhibitors enhance antitumor efficacy and persistence of CAR-T cells by activation of the Wnt pathway. Cell Rep. 2024;43(4):114065.

Publisher's Note